Unravelling Gas-Particle Partitioning Dynamics in Cooking Aerosol Oxidation through Non-Targeted FIGAERO-CIMS Analysis

Ruizhe Shen[1], Song Guo[1,2]*, Hui Wang[1], Ying Yu[1], Zichao Wan[1], Rui Tan[1], Wenfei Zhu[1], Zheng Chen[1], Shiyi Chen[1], Zhijun Wu[1], Shuangde Li[3], Yunfa Chen[3], Min Hu[12]

[1]State Key Laboratory of Regional Environment and Sustainability, International Joint Research Center for Atmospheric Research (IJRC), College of Environmental Sciences and Engineering, Peking University, Beijing, 100871, China
[2]Collaborative Innovation Centre of Atmospheric Environment and Equipment Technology, Nanjing University of Information Science & Technology, Nanjing, 210044, China
[3]State Key Laboratory of Multiphase Complex Systems, Institute of Process Engineering, Chinese Academy of Sciences, Beijing, 100190, China

Correspondence to: Song Guo (songguo@pku.edu.cn)

Abstract. Cooking emissions are increasingly important sources of organic aerosol in densely populated urban areas as clean-air actions reduce emissions from industrial activities and fossil-fuel combustion. Their atmospheric evolution and environmental and health effects remain difficult to assess because of the complexity of their composition and transformation pathways. Here, we conducted a laboratory study of emissions from heated corn oil using a Go:PAM oxidation flow reactor. We investigated the evolution of composition, volatility, and gas-particle partitioning and evaluated discrepancies between FIGAERO-based measurements and thermodynamic estimates. FIGAERO-I-CIMS measurements combined with a 2-D VBS parameterization were used to characterize the composition and volatility distributions of primary and secondary cooking-originated organic aerosol. Kinetic calculations indicate molar-weight-dependent partitioning kinetic schemes with surface process as rate-limiting step. Partitioning of primary cooking aerosols is generally biased toward gas phase compared to the equilibrium state. In secondary aerosol, partition of compounds with molar mass under 120 g/mol favours gas phase, compounds between 120-220 g/mol exists in near-equilibrium state, species with molar mass over 220 g/mol favours aerosol phase. The thermodynamic comparison nevertheless reveals a substantial unresolved gap between FIGAERO-derived effective volatility and equilibrium thermodynamic estimates, reflecting combined measurement and model uncertainties. Results clarify the scope of kinetic limitations in gas-particle partitioning during cooking-emission and oxidation, identify priorities for improving the representation of cooking emissions in atmospheric studies.

1 Introduction

Secondary organic aerosol (SOA) is a major component of atmospheric submicron particulate matters on both global and regional scales. (Hallquist et al., 2009) Anthropogenic SOA is particularly prominent in densely populated regions because of the strong influence of human activities on its precursor emissions, thus counteracting on urban environment and human health(Guo et al., 2020). While emissions from industrial and transportation sectors have been increasingly regulated

under clean-air initiatives, cooking emissions which vary with culinary and cooking practicesare emerging as significant sources of atmospheric volatile organic compounds (VOCs), semi-volatile and intermediate-volatile organic compounds (S/IVOCs), and SOA precursors. Moreover, cooking represents a persistent source of indoor emissions in households, catering facilities, and restaurants, and accounting for over 20% of indoor activity time. Notably, exposure to indoor SOA formation may pose significantly greater health risks than to outdoor SOA in urban settings, given the substantial amount of time people spend indoors. Additionally, cooking emissions exhibit high spatial heterogeneity across urban areas, with emission profiles and environmental impacts varying considerably by regional culinary practices, leading to substantial uncertainties in emission estimates(Zhu et al., 2021). Therefore, effective clean-air policies aimed at mitigating cooking emissions require accurate and precise quantification and characterization of both emissions and atmospheric transformation pathways.

Current research on cooking emissions has primarily focused on characterizing the gas- and particle-phase composition of primary cooking emissions, along with variations linked to culinary practices. Key factors include cuisine and cooking style, ingredient composition (including food ingredients and cooking-oil type), and cooking conditions (e.g., oil temperature and the use of seasonings),which is unlike standardized industrial or transportation emissions (Rogge et al., 1991; He et al., 2004; Zhao et al., 2007; Li et al., 2015) Gas-phase cooking emissions is dominated by short-chain carbonyls and aliphatic acids, whereas the particle phase is rich in long-chain aliphatic acids. Other weakly oxygenated species derived from thermal decomposition and ingredient–oil interactions—such as sterols and polycyclic aromatic hydrocarbons (PAHs)also contribute significantly to aerosol composition(Lin et al., 2021). These emissions exhibit substantial SOA formation potential in urban, suburban, and even indoor environments. (Zeng et al., 2020; Guo et al., 2023) However, the gas-particle partitioning of organic compounds during the transformation of cooking emissions remains poorly understood, primarily due to the complexity and dynamic evolution of organic composition throughout emission and aging processes. This knowledge gap represents a major challenge in atmospheric chemistry. Since gas-particle partitioning directly influences the environmental and health impacts of both primary and secondary organic aerosols, understanding on detailed mechanism within evolution processes of organic aerosols is essential for accurate risk assessment and effective air quality management.

High variety of primary organic species and complex secondary transformation process led to diverse emission and evolution characteristics(Zeng et al., 2020; Zhu et al., 2021; Tan et al., 2023; Lu et al., 2024). While most techniques rely on chromatographic separation to achieve high chemical resolution, thus temporal resolution remains limited (Song et al., 2023; Yang et al., 2023). Moreover, despite increasing characterization of primary cooking emissions and cooking-derived SOA, the molecular-level evolution of gas–particle partitioning during oxidation remains poorly understood. Previous studies have largely focused on the chemical composition of primary emissions or on bulk properties of secondary cooking aerosol, whereas molecularly resolved constraints on the thermodynamics and kinetics of gas–particle partitioning remain limited (Takhar et al., 2019; Takhar et al., 2021; Masoud et al., 2022; Kristensen et al., 2023; Sun et al., 2026).Here, we combine gas- and particle-phase measurements by FIGAERO coupled with chemical ionization mass spectrometry (FIGAERO-CIMS) with 2-D VBS analysis, positive matrix factorization, and thermodynamic and kinetic calculations to investigate the

oxidation of cooking emissions. Specifically, we examine how molecular composition, volatility, and gas-particle partitioning evolve with OH exposure and evaluate the extent to which the observed partitioning behavior can be described by thermodynamic equilibrium and characteristic mass-transfer timescales . This study will give a comprehensive insight into gas-particle partitioning thermodynamics and kinetics based on PMF analysis and thermodynamic estimations.

2 Materials and methods

2.1 Experimental setup

Oxidation experiments of cooking emissions were conducted in a domestic lifestyle emission laboratory utilizing a Go:PAM Oxidation flow reactor (OFR) (Wang et al., 2021). Detailed experimental setup is provided in previous works of our research group (Yu et al., 2022; Tan et al., 2023). Briefly, Go:PAM reactor was operated under mode OFR254, in which OH radical are generated by the reaction between $O(^1D)$ radicals and water vapor. OFR254 represent atmospheric oxidation processes dominated by OH radical under the low to medium NO_x conditions in this study(Peng and Jimenez, 2020). OH exposure in the Go:PAM system is controlled by varying ozone concentration, relative humidity, and the experimental sample gas flow rate through the Go:PAM reactor, and estimated using semi-empirical parametrizations in OFR254 recommended by Peng et al., based on measured OH reactivity, ozone concentration and relative humidity (Peng et al., 2016). Cooking experiments were performed in a custom-made fry pan directly connect to pure nitrogen as carrier gas to avoid interference of high NO_x in ambient air on radical oxidation and I-CIMS detection. Cooking emissions are generated by heating corn oil to 120~130 ℃, a temperature range selected to represents domestic oil-heating conditions and, to some extent, frying and stir-frying practices within typical domestic cooking activities that are widely used in both Eastern and Western cooking types(Rogge et al., 1991; He et al., 2004; Abdullahi et al., 2013; Bandowe et al., 2021). Four replicate experiments were performed to assess reproducibility.. It should be noted that this experiment represents a controlled, low-NOx oil-heating case rather than the full range of cooking emissions, thus the results should not be directly extrapolated to NOx-rich cooking plumes. It should be noted that, OFR utilization in oxidation simulation experiments can introduce OH suppression, altered RO_2 chemistry, causing secondary photolysis, and resulting in enhanced fragmentation; thus, the chemical environment of oxidation in Go:PAM might differ from that of real atmosphere, e.g. the OH-exposure-to-atmospheric-age conversion is used only as an approximate reference(Peng and Jimenez, 2020). Detailed experimental conditions and setup are presented in **Section S1, Supplement Information 1**.

2.2 Instrumentation

The instrumentations used in this study consist of three categories, including oxidation conditions, gas-phase organic composition, aerosol size and mass, and gas- and particle-phase molecular composition and volatility. For oxidation conditions in the Go:PAM reactor, ozone concentration are monitored using Thermo® model 49i ozone analyzer. Organic species in the gas phase, including precursors and low-molecular-weight oxidation products, are quantified on-line using

Vocus-PTR instruments. Aerosol size distribution before and after entering Go:PAM is measured by two Scanning Mobility Particle Sizer (SMPS) systems. The upstream SPMS before Go:PAM consists of a TSI® model 3080 DMA with a model 3776 CPC, and the downstream SMPS comprised a model 3082 DMA and a model 3772 CPC. Particle density measurement adopted Cambustion® Centrifugal Particle Mass Analyzer (CPMA) for total mass estimation at various OH exposure level(Zhao et al., 2007; Zhang et al., 2020; Abdullahi et al., 2013). Molecular composition, gas-particle partitioning, and volatility of organic aerosols and are determined by a FIGAERO inlet coupled to HR-ToF-CIMS instrumentation developed by Aerodyne Inc® that choose iodide as reagent ion. Operation of FIGAERO-CIMS instrument in laboratory oxidation experiments has been elaborated since the instrumentation were firstly developed (Lopez-Hilfiker et al., 2014; Le Breton et al., 2019; Bannan et al., 2019). Briefly, the FIGAERO inlet consists of a gas-phase sampling inlet that pull air directly into the API interface and IMR of CIMS instrument, and an aerosol inlet that collect aerosol samples onto a PTFE filter. One analyzes cycle is completed by a 15-min gas-phase inlet sampling period when particles collected onto the filter at aerosol inlet, a 15-min particle phase thermal desorption period when 320 ℃ heated air for thermal desorption flush through the filter and increase filter temperature linearly from room temperature to 180 ℃, a 15-min continuous heating scheme for completing aerosol sample desorption, and a 15-min cooling scheme. FIGAERO inlet provides the possibility of determining both gas phase and particle phase concentration, and thus gas-particle partitioning information combined with high-resolution composition data acquired by CIMS instrumentation (Lopez-Hilfiker et al., 2016). Gas-particle partitioning coefficient K_p, defined similar to phase- equilibrium coefficients between gas-phase and particle-phase organic species, is determined from paired- average CIMS signal in gas-phase and aerosol-phase, and OA concentration determined by SMPS system. Particle-phase volatility was inferred from FIGAERO thermograms obtained during thermal desorption, using the relationship between thermogram peak temperature (T_{max}) and effective saturation vapor pressure(Bannan et al., 2019). Sensitivity and volatility calibrations have been proceeded adopting certain authentication standards relevant in primary and secondary cooking emissions and following atmospheric transformations (Ylisirniö et al., 2021).Sensitivities for species without corresponding reference standards were estimated using an in-house composition-based parameterization. Note that Iodide-CIMS is selective toward polar and oxygenated compounds and may underrepresent weakly oxygenated or nonpolar material, thus instrumental-selection-based measurement uncertainties would be taken into account in the following analysis. Accordingly, the molecular-composition and 2-D VBS distributions reported here characterize the iodide-CIMS-detectable ion population rather than providing mass-complete representation of all cooking emissions(Iyer et al., 2016). Trace sulfur-containing formulas were not used for mechanistic source interpretation because the corn-oil-only experiment contained no sulfur-rich food ingredients and the low-abundance signals may reflect background, contamination, or formula-assignment uncertainty(Zhang et al., 2020; Song et al., 2022). Detailed operation and data process of various instruments, sensitivity and volatility calibration methods, and quantification of species without authentication standard are presented in **Section S2, Supplement S1**.

2.3 Two-Dimensional Volatility Basis Set (2-D VBS) framework construction

The Two-Dimensional Volatility Basis Set (2-D VBS) framework has been developed to characterize the complex composition of organic aerosols in laboratory experiments, ambient observations, and modeling studies. 2-D VBS approach maps organic species onto a two-dimensional space defined by carbon oxidation state (Donahue et al., 2011; Donahue et al., 2012; Chuang and Donahue, 2016). Gas- and particle-phase composition and gas-particle partitioning parameters (partitioning coefficients K_p) of primary emissions and secondary oxidation experiments are thus mapped in 2-D VBS space, to intuitively visualized the composition characteristic and evolution of organic aerosol and its gas-particle partitioning characteristics. Saturation vapor concentration in the 2-D VBS space are estimated from molecular formula assigned by I-CIMS detection using an empirical parameterization recommended by Li et al. (Li et al., 2016). Detailed adoption of 2-D-VBS approach is shown in **Section S3, Supplement Information 1**.

2.4 Positive-Matrix-Factorization (PMF) analysis

HR-ToF-CIMS enables the detection of thousands of ions, corresponding to a comparable number of chemical species. In the present study, the FIGAERO-CIMS instrument detected 936 assignable ions corresponding to specific compounds in both gas phase and secondary organic aerosol (SOA). Complex feature of cooking aerosols and atmospheric evolution required adoption of deconvolution methods to extract interpretable composition and volatility patterns from the complex dataset of experimental concentration profiles, and to select representative species from species at various oxidative exposure in oxidation of cooking aerosols. In this study, we proceeded various factorization and data pre-treat methods, and choose Positive Matrix Factorization (PMF) via the Igor Pro®-based SoFi® ME-2 PMF software (Canonaco et al., 2013; Buchholz et al., 2020a). In addition, ordinal analysis methods previously established by Kong et al. was further used to identify the most abundant and representative ions within each resolved factor. (Kong et al., 2021). Detailed factorization method assignments are shown in **Section S4, Supplement Information 1.**

2.5 Gas-particle partitioning thermodynamics and kinetics

Gas-particle partitioning thermodynamics of cooking organic aerosols are discussed comparing FIGAERO measurements and theoretical estimation. Estimated gas-particle partitioning parameters are estimated based on absorption partitioning theory and compared to FIGAERO concentration measurements(Pankow, 1994). Experimental K_p values are derived from paired FIGAERO gas- and particle-phase measurements together with the measured organic-aerosol mass concentration reported in Table S6.1. For the equilibrium calculation, the organic mass fraction is assumed to be unity, the mean molecular weight of the particle-phase organic material was calculated as a concentration-weighted average over the detected molecular composition. For fingerprint species extracted from CIMS detection based on PMF and ordinal analysis(Buchholz et al., 2020b; Kong et al., 2021), saturation vapor pressure are estimated utilizing SIMPOL(Pankow and Asher, 2008), and activity coefficients are calculated using group-contribution method AIOMFAC. To ensure whether

liquid-liquid phase separation will occur within cooking POA and SOA, , aerosol phase molar-fraction based activity are calculated (Zuend and Seinfeld, 2012) (https://aiomfac.lab.mcgill.ca/). A Kelvin effect correction is adapted assuming a typical organic aerosol surface tension of 0.05 N m^{-2}(Cai and Griffin, 2003; Schmedding et al., 2025). Gas-particle partitioning kinetics are discussed accounting for gas-phase diffusion, aerosol-phase diffusion, surface accommodation and particle coagulation. We calculate the characteristic time τ of processes in gas-particle partitioning, compared them with retention and oxidation times in the Go:PAM flow tube. Detailed gas-particle partitioning schemes are shown in **Section S5, Supplement Information 1**.

3 Results and discussion

3.1 Size & mass Distributions evolution of cooking organic aerosols in oxidation process

The evolution of particle size and mass distributions from primary to secondary cooking aerosols with increasing OH exposure was shown in **Figure 1**. Detailed size and mass distribution characteristics of aerosols are shown in **Table S6.1**, **Supplement S1.** Primary cooking aerosols exhibit a relatively broad size distribution, with particle diameters ranging from 50 to 300 nm. can originate from evaporation of oil constituents followed by condensation, as well as from thermally induced oxidation and decomposition reactions. Primary cooking aerosols comprise of components with large molecular size and relatively low carbon oxidation states, such as long-chain alkanes, alkenes, alkanals, alkenones, fatty acids and their glycerol esters, and steroids(Rogge et al., 1991; Nolte et al., 1999). In contrast, secondary particles exhibited a predominantly unimodal size distribution, with modal diameters below 50 nm. Both particle number and mass concentrations increased rapidly upon OH oxidation. Both particle number and mass concentrations increased rapidly upon OH oxidation, even at the lowest investigated OH exposure, the lowest OH concentration conditions, secondary aerosol number concentrations can reach up to 10^6 # cm^{-3}. Mode diameter of SOA increased from 14.1nm to 31.1nm with enhancement of OH exposure from ~10^9 to 10^{10} # cm^{-3} s, accounting for particle mass growth factor of $(31.1/14.1)^3$~10, while total number concentration increases from 1.37 to 3.42×10^6 # cm^{-3}, accounting for particle mass growth factor of ~2.5. Moreover, as OH exposure growth, the number concentration of nuclear mode (d_p<20nm) decreases from 9.61 to 7.66×10^5 # cm^{-3}, mass concentration is kept around 1.75~2 μg·m^{-3}. Evolution of Size and mass distribution with enhancement of OH exposure indicate that increasing OH exposure further enhances mass concentration predominately through particle size growth rather than number increase, implying that the dominate driving force of SOA growth is condensation of gas-phase products, while formation of new particles serve as initialization process of SOA formation and growth. For particles larger than 90 nm where primary aerosols are most abundant in, enhancement of OH exposure result in minimal changes in number and mass concentration, with average declination of less than 20% even under the highest OH exposure conditions (**Fig. S6.1**, **Supplement S1**). These findings collectively suggest that secondary organic aerosols from oil boiling originate mainly from condensation of gas-phase oxidation products to form nucleation and Aitken mode particles, rather than oxidative aging and modification of primary aerosols in accumulation mode(Tan et al., 2023; Zhang et al., 2023). The observed low reactivity of

primary cooking aerosols during oxidation may be attributed to the low miscibility between nonpolar or low-polarity primary components and newly formed highly polar secondary compounds likely resulting from limited partitioning tendency of primary components, or lower number concentration and specific surface area of primary aerosols from oil-boiling activities than secondary cooking aerosols even at the lowest OH exposure, leading to limited gas-particle partitioning rate(Chandramouli et al., 2003; Milsom et al., 2021; Liu et al., 2025) ,.

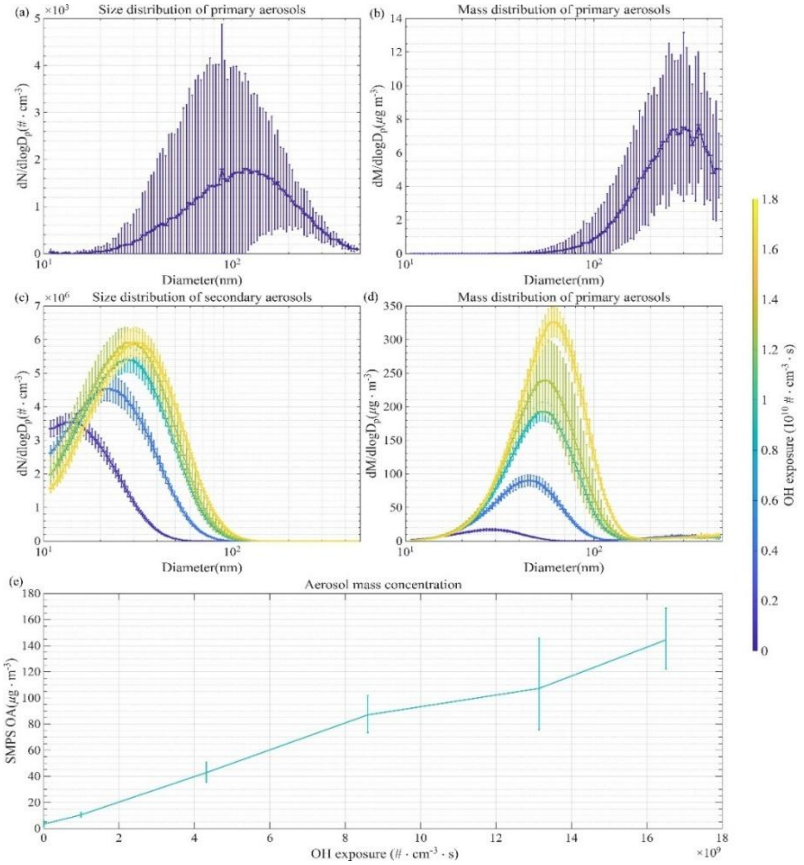

Figure 1 Primary and Secondary aerosol size & mass distribution evolution with OH exposure increases. (a) (b)illustrate size and mass distribution of primary particles, (c) (d) size and mass distribution of secondary aerosols at OH exposure 0.1~1.8 ×10^{10} cm^{-3} s. (e) exhibits mass concentration evolution with oxidation process from primary to OH exposure 1.8 ×10^{10} cm^{-3} s.

3.2 Composition and volatility distribution of primary and secondary organic aerosols in 2-D VBS Space

The volatility and compositional distribution of cooking aerosols and associated gas-phase organic components within the two-dimensional volatility basis set (2-D VBS) framework (Donahue et al., 2012) were displayed in **Figure 2**. Average composition and volatility evolution are shown in **Table 1**. Most detected species fell within the S/IVOC range and had $\overline{OS_c}$ between approximately –1.25 to 0.5. Throughout the oxidation experiment, increasing OH exposure led to a substantial enhancement of S/IVOC components, consistent with the trend observed for aerosol particles. Additionally, the

formation of low-volatility, highly oxidized compounds (classified as LVOC) derived possibly from multi-generation oxidation is also promoted.

In gas phase, the average molecular size increases significantly during oxidation, whereas the carbon oxidation state remains nearly constant or exhibits a slight decrease following OH radical addition. This behavior may be attributed to the formation of gas-phase oxidation products via cleavage of long-chain fatty acids, polymerization among oxidation intermediates such as RO_2 and RO radicals, and the oxidative depletion of primary low-molecular-weight organic acids resulting from glycerol thermal decomposition, such as formic acid, acetic acid, and glyceric acid (Zhang et al., 2018; Takhar et al., 2022). By contrast, compositional shifts in the aerosol phase within the 2-D VBS space—such as in oxidation state and molecular size—are relatively minor compared to those in the gas phase. The oxidative state changes of particle-phase organics with enhanced OH exposure is relatively minor, with only marginal growth in molecular dimensions. The relatively small molecular size of primary cooking aerosols may result from the limited detection sensitivity of iodide-adduct CIMS toward nonpolar or low-polarity compounds with large molecular weights and fewer oxygen-containing functional groups, e.g., long-chain hydrocarbons, fatty acids, and steroids (Iyer et al., 2016). These compositional patterns suggest that gas-phase oxidative formation and condensation of secondary gas phase S/IVOCs onto SOA particles would serve as a more predominately source of SOA formation and growth, rather than by continuous oxidation within the particle phase. Observation implies that the oxidation process in the flow tube would have been approaching a "steady-state turning point" with enhancement of OH exposure because of the formation of higher-oxidized and lower-volatile oxidation products. These products, formed through oxidation of long-chain primary acids and carbonyls, exhibit lower volatility, higher viscosity and lower oxidation rate, thereby slowing subsequent oxidative aging (Milsom et al., 2021). Particle-phase products reach this stage earlier owing to their oxygen-rich nature, such as major abundance of $C_{>6}$ dicarboxylic acids and peroxides. The somewhat close average volatility between gas-phase and aerosol phase would possibly show underlying kinetic and thermodynamic mechanisms. Note that measurement and estimation uncertainty of FIGAERO-CIMS and 2-D-VBS, including thermal decomposition, might influence the results. Detailed 2-D VBS distribution of primary and secondary organic matter in gas and aerosol phase are shown in **Supplementary Material S2**.

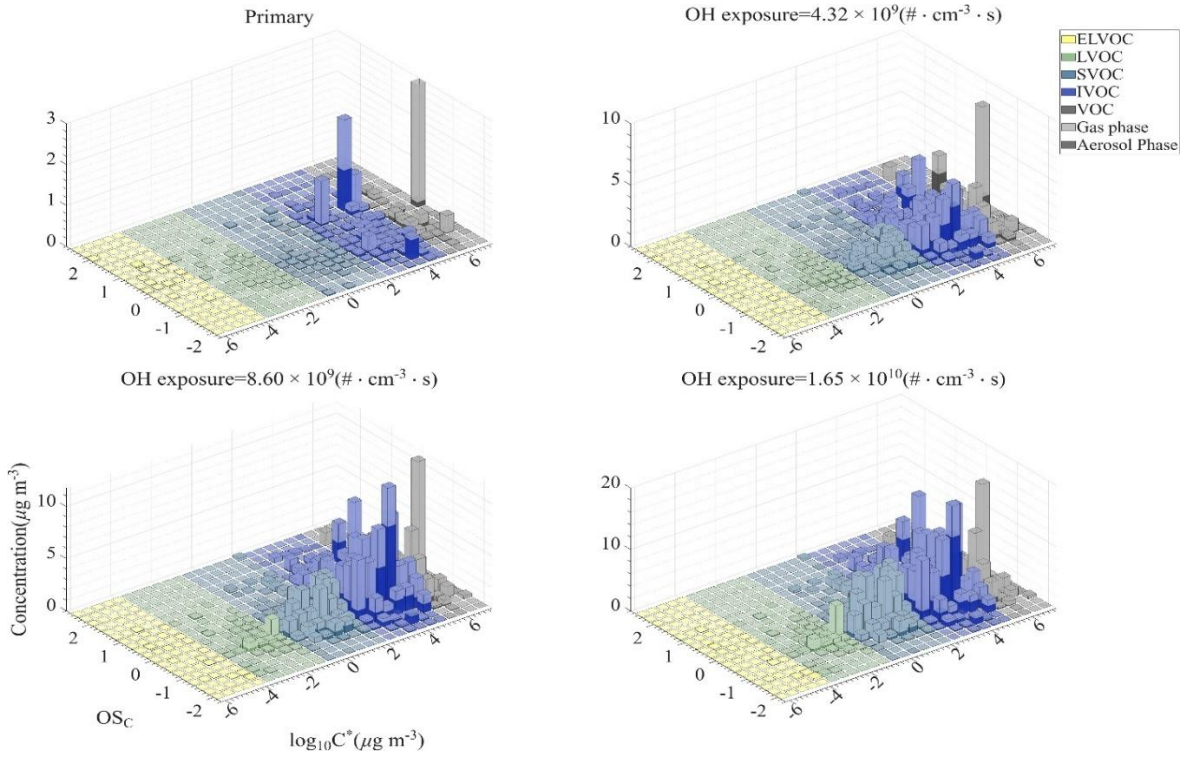

Figure 2 Distribution of gas-phase and aerosol-phase primary and secondary cooking organic species in 2-D VBS space with oxidation

Table 1 Average molecular composition and volatility parameters of primary and secondary organic components in gas phase and aerosol phase

OH exposure (cm^{-3} s)	Molecular composition	$\log_{10}C^0(\mu g \cdot m^{-3})$	OS_C
Primary	$C_{3.5}H_{5.4}O_{2.6}N_{0.03}S_{0.01}$*	6.0*	-0.11*
	$C_{7.1}H_{10.3}O_{3.8}N_{0.09}S_{0.03}$**	2.8**	-0.47**
4.32×10^9	$C_{5.8}H_{9.5}O_{3.7}N_{0.07}S_{0.04}$*	3.5*	-0.45*
	$C_{7.3}H_{11.9}O_{3.8}N_{0.04}S_{0.01}$**	2.8**	-0.63**
9.60×10^9	$C_{6.6}H_{10.6}O_{4.0}N_{0.07}S_{0.05}$*	2.8*	-0.49*
	$C_{7.8}H_{12.9}O_{4.0}N_{0.04}S_{0.01}$**	2.4**	-0.67**
1.65×10^{10}	$C_{7.0}H_{11.0}O_{4.2}N_{0.07}S_{0.06}$*	2.3*	-0.47*
	$C_{7.8}H_{13.0}O_{4.1}N_{0.04}S_{0.01}$**	2.2**	-0.65**

* Gas phase **Aerosol phase

3.3 Classification and Quantification of Primary and Secondary Cooking Emissions by PMF Analysis

ME-2 PMF methods are adopted in deconvolution and non-targeted analysis of FIGAERO-CIMS detections on gas-phase and aerosol-phase organic compounds with different volatility and oxidative state, so as to classify typical organic species, and extract evolution pattern corresponding to oxidation mechanism and changes of gas-particle partitioning from complex CIMS data matrix (Buchholz et al., 2020b; Hashimoto et al., 2022; Kong et al., 2021). Detailed PMF recommended factor determination methods are shown in **Section S4 of Supplement S1**. **Figure 3** shows the optimized ME-2 PMF results of FIGAERO-CIMS data. 13 factors were interpreted according to their phase distribution, volatility, oxidation state, and evolution with OH exposure, whereas the remaining factor was assigned as a background/interference factor. Factors are listed in **Fig. 3** and classified by its volatility (partitioning coefficient K_p while total amount is countable) and oxidative state (mean oxidative state OS_C and evolution with enhancement of OH exposure). Detailed factor classification and interpretation procedure is shown in **Section S4 of the Supplement S1**. Formic acid (at m/z 173, detected as $ICH_2O_2^-$ in CIMS) are not included in PMF analysis due to its extreme high abundance in gas phase primary emissions and low oxidative states compared to other species (up to 25ppb, shown in **Fig. S6.3**), and would be separately discussed here. High abundant of formic acid at ppb in indoor sources and cooking emissions at ppb level has been reported in previous researches on cooking emission (Reyes-Villegas et al., 2018; Farmer et al., 2019). Formation of cooking originated formic acid possibly due to thermal decomposition of glycerol in primary species; The relative fragile structure of glycerol-related skeleton(e.g. glycerol, lactic acid, acrylic acid, and pyruvic acid) would favor the formation of formic acid originated from thermal oxidation and decomposition, leading to high abundance of formic acid in gas-phase primary emissions (Nolte et al., 1999; Farmer et al., 2019; Zhang et al., 2021; Takhar et al., 2022; Ye et al., 2012). Primary formic acid would decline slower than estimated from OH radical reactivity (formic acid decline about 22% at OH exposure ~10^{10} cm^3 s^{-1}) at OH exposures in current research (Farmer et al., 2019; Atkinson et al., 2006), indicating secondary source of formic acids, possibly by ozonolysis of unsaturated compounds and further oxidation of glycerol-related species(Farmer et al., 2019; Takhar et al., 2021; Zhang et al., 2021).

Among factors, we would first classify the 13th factor as more closely to a background factor as shown in **Fig. S6.4** due to unreasonable thermogram including ill-shaped multiple distinct peaks at different desorption temperature. This factor is named Background, apart from other factors classified by volatility and oxidative states. Intensity of factor Background is relatively low, showing that contaminant would not be able to interfere measurement result too much. Among reasonable factors, V-Pri (**Figure S6.5**) and SV-Pri (**Figure S6.8**) are classified as primary emissions. The average elemental composition and most abundant species of V-Pri and SV-Pri are shown in **Table S6.2-S6.3**. Factor V-Pri stands for gas-phase primary emission, mainly consist of low-molecular-weight oxygenated organic compounds such as short chain carboxylic acids and their deviates(Masoud et al., 2022; Ye et al., 2012; Zhang et al., 2021). Most abundant compounds in Factor V-Pri are $C_{1\text{-}3}$ oxygenated organic species, such as $C_3H_4O_2I^-$ (m/z 198.93, iodide adduct, **Figure S6.6**) corresponding to acrylic acid, $C_2H_4O_2I^-$ (m/z 186.92, iodide adduct) corresponding to acetic acid, $C_3H_8O_3I^-$ (m/z 218.95, iodide adduct)

corresponding to glycerol. These compounds probably originate from thermal oxidation or thermal decomposition of glycerol, which are formed by thermal decomposition of oil esters (Nawar, 1969; Nolte et al., 1999; Martins et al., 2013; Lopez-Pedrajas et al., 2018; Reyes-Villegas et al., 2018). Lesser abundant compounds in V-Pri are larger less-oxygenated compounds with carbon number >5 and oxygen number ≤2, probably formed from thermal decomposition of fat followed by thermal oxidation processes long-chain aliphatic acids, including $C_6H_{12}O_2I^-$ (m/z 242.99, iodide adduct, **Figure S6.7**) corresponding to hexanoic acid and $C_5H_{10}O_2I^-$ (m/z 228.97, iodide adduct) corresponding to pentatonic acid (Takhar et al., 2022; Takhar et al., 2021; Nolte et al., 1999; Qian et al., 2026; Xiao et al., 2023). Semi-volatile factor SV-Pri contains semi- and intermediate- volatile organic compounds with medium carbon number (5 carbons on average) and higher oxidative state than V-Pri. Most abundant compounds are $C_{3\text{-}6}$ and $O_{2\text{-}3}$ compounds, which may correspond to organic acid derivatives, such as hydroxy-carboxylic acids and carbonyl-carboxylic acids that originate from thermal oxidation of long-chain aliphatic acid in primary emissions. Compound detected as $C_5H_4O_4I^-$ (m/z 254.91, iodide adduct, **Figure S6.11**), possibly corresponding to furan-structure compounds such as aconic acid or hydroxy furoic acid, has the highest intensity in SV-Pri. $C_5H_4O_4$ present mostly in gas phase during primary emission, while particle-phase abundance increases with oxidation age increasing, indicating its possible primary thermal oxidation and dehydration origin, leading to gas-phase degradation and partitioning toward aerosol phase while SOA concentration significantly increases(Kawada et al., 1967; Nawar, 1969; Grebenteuch et al., 2021; Xiao et al., 2023; Yao et al., 2024; Hou et al., 2025). Other typical compounds abundant in SV-Pri with similar evolution characteristics includes long-chain aliphatic acids, such as palmitic acid ($C_{16}H_{32}O_2I^-$, m/z 383.14, iodide adduct, **Figure S6.9**), oleic acid ($C_{18}H_{34}O_2I^-$, m/z 409.16, iodide adduct, **Figure S6.10**). These typical primary organic compounds have evolution trends similar to $C_5H_4O_4$, with increasing are apparently abundant in gas phase and aerosol phase, but with lower concentration than small molecules ones, probably due to the quantification uncertainty of sensitivity estimation of lower-oxygenated long-chain organics(Lee et al., 2014; Chiaia et al., 2024; Zhou et al., 2022). Gas-particle partitioning of other typical species mostly abundant in factor SV-Pri such as $C_5H_8O_3I^-$ (m/z 254.91, iodide adduct, **Figure S6.12**) show different evolution pattern other than primary compounds, implementing two distinct origins of these compounds: primary formation from gas-phase thermal oxidation, and secondary formation from oxidation of primary emissions(Zeng et al., 2020; Masoud et al., 2022; Yao et al., 2024).

Factors with intermediate oxidative state, including V-OxiGen^{1st}-Gly, V-OxiGen^{1st}-FA, SV-OxiGen^{1st} and LV-OxiGen^{1st}-Gly^{TD} (**Figures S6.13-16**), achieve highest abundance at medium oxidative exposure. Among these factors, V-OxiGen^{1st}-Gly and LV-OxiGen^{1st}-Gly^{TD} are factors with smaller molecular size, reach its peak concentration at lower OH exposure, while V-OxiGen^{1st}-FA and SV-OxiGen^{1st} reaches maximum at higher oxidative state and contains larger molecules. Typical volatile intermediate -oxidative-state factor V-OxiGen^{1st}-Gly mainly consist of two distinct categories of species. The first is $C_{2\text{-}3}$ oxygenated compounds that are higher-oxidized than corresponding compounds abundant in V-Pri, such as $C_3H_4O_3I^-$ (m/z 214.92, iodide adduct, possibly pyruvic acid, **Figure S6.6**) and $C_2H_4O_4I^-$ (m/z 214.92, iodide adduct, **Figure S6.17**) that may originate from first-generation OH oxidation or ozonolysis of glycerol-related compounds. The other is $C_{4\text{-}7}$ oxygenated compounds at intermediate oxidative exposure with medium oxidative state, such as $C_5H_{10}O_3I^-$ (m/z

244.97, iodide adduct, **Figure S6.18**) and $C_7H_{12}O_3I^-$ (m/z 214.92, iodide adduct, **Figure S6.20**), corresponding to first-generation fragmentation product of long-chain fatty acids during OH and ozone oxidation, or ozonolysis, or first-generation thermal oxidation products(Takhar et al., 2021; Takhar et al., 2022; Liu et al., 2024). Factor LV-OxiGen^{1st}-Gly^{TD} have similar average oxidative state and molecular size with V-OxiGen^{1st}-Gly, seems corresponding to gas phase portion of first-generation oxidation products represented by V-OxiGen^{1st}-Gly. However, thermal desorption thermogram of LV-OxiGen^{1st}-Gly^{TD} peaks at ~440K, showing that compounds represented by LV-OxiGen^{1st}-Gly^{TD} have much lower volatility than molecular composition corresponding to this factor, indicating that LV-OxiGen^{1st}-Gly^{TD} representing thermal decomposition fragmentations of oxidation products with long-chain fatty acid structure (Frankel et al., 1983; Patrikios et al., 1994; Martins et al., 2013; Aladedunye, 2016; Bonetti and Parker, 2019; Lopez-Hilfiker et al., 2019; Zeng et al., 2020; Brown et al., 2021), whose actual species may have elemental composition of $C_{16/18}H_{30-34}O_{3-6}$. Particle-phase reactions between possible peroxides (such as $C_7H_{12}O_5$ and $C_9H_{16}O_5$ that abundant in V-OxiGen^{1st}-Gly and LV-OxiGen^{1st}-Gly^{TD}) and substituted alcohols or aldehydes ($C_6H_{12}O_3$ or $C_6H_{10}O_3$, etc.) accelerated in thermal desorption at lower oxidative stage may also be an alternative source(Luo et al., 2024; Qian et al., 2026). Volatile factor V-OxiGen^{1st}-FA and semi-volatile factor SV-OxiGen^{1st} share similar molecular composition such as overall oxidation state, molecular size and typical species. These species, mostly C_{4-6} acids in gas phase and C_{9-10} carbonyl acids in aerosol phase, have larger molecular size. These factors are totally generated from oxidation of fatty acids rather than compounds related to glycerol that are abundant in lower-oxidative-exposure factors. Moreover, comparing thermal desorption properties with molecular composition, species in Factor SV-OxiGen^{1st} represent compounds with exact molecular formula detected by CIMS rather than thermal decomposition products(Reyes-Villegas et al., 2018; Masoud et al., 2022; Takhar et al., 2021). Overall, Typical intermediate compounds are pyruvic acid in gas phase, C_{5-10} carbonyl acids in both phase and large-molecular oxidation products $C_{16/18}H_{30-34}O_{3-4}$ in the aerosol phase.

Highly-oxygenated factors include volatile factors V-MultiGen-Gly and V-MultiGen-FA, semi-volatile factor SV-MultiGen-peroxy, low-voaltile factors LV-Multigen-HMW, LV-Multigen-COOH, LV-Multigen-peroxy (**Figures S6.26-31**). These factors reach highest intensity at highest experimental oxidative exposure. Among factors, V-MultiGen-Gly and LV-Multigen-HMW are lesser oxidized, the amount of these factors reaches steady state while oxidative exposure increases to maximum in the experiment. Other factors are highly oxidized: their abundance increases significantly during oxidative exposure growth. Typical gas phase species are highly oxidized termination products of glycerol-related species, such as $C_3H_4O_4I^-$ (m/z 230.91, iodide adduct, probably malonic acid, **Figure S6.19**) and $C_3H_6O_4I^-$ (m/z 232.93, iodide adduct, probably glyceric acid), or low-molecular-weight fragmentation products of fatty acid oxidation, such as $C_4H_6O_4I^-$ (m/z 244.93, iodide adduct, probably succinic acid, **Figure S6.33**) and $C_6H_{10}O_4I^-$ (m/z 244.93, iodide adduct, probably adipic acid, **Figure S6.32**). These highly oxidized low-molecular weight compounds are more semi-volatile rather than volatile species(Zeng et al., 2020; Masoud et al., 2022; Takhar et al., 2021). Aerosol phase compounds are mostly $C_{7-10}H_{12-16}O_{4-6}$ compounds that may corresponding to C_{7-10} organic acids, diacids, and its derivates. Typical species include $C_9H_{16}O_4I^-$ (m/z 315.01, iodide adduct, probably azelaic acid **Figure S6.37**), $C_9H_{18}O_4I^-$ (m/z 317.03, iodide adduct, possibly dihydroxy or

hydroperoxyl C_9 carboxylic acid), and $C_{10}H_{18}O_4I^-$ (m/z 329.03, iodide adduct, possibly sebacic, **Figure S6.38**). Highly oxygenated species with 5 oxygen atoms and more are abundant in those low-volatile factors compared to intermediate-oxidative state factors, including $C_{10}H_{18}O_5I^-$ (m/z 329.03, iodide adduct, possibly C_{10} hydroperoxyl carboxylic acid, **Figure S6.39**) and $C_9H_{16}O_5I^-$ (m/z 329.03, iodide adduct, possibly C_9 hydroperoxyl carboxylic acid, **Figure S6.40**)possibly corresponding to hydroperoxyl deviates of carboxylic acids(Zhou et al., 2022; Takhar et al., 2022; Grebenteuch et al., 2021; Yao et al., 2024). Highly-oxygenate products $C_{16/18}H_{30\text{-}34}O_{\geq 5}$ (**Figure S6.35-36**)are auto-oxidation products that keep long-chain fatty acid structure, abundant in factor LV-Multigen-HMW(Shilling et al., 2019; Takhar et al., 2019; Patrikios et al., 1994; Du et al., 2025).These larger molecule multi-generation auto-oxidation products have similar or slightly higher oxidative state and lower saturation vapor pressure, thus are more abundant in the aerosol phase.

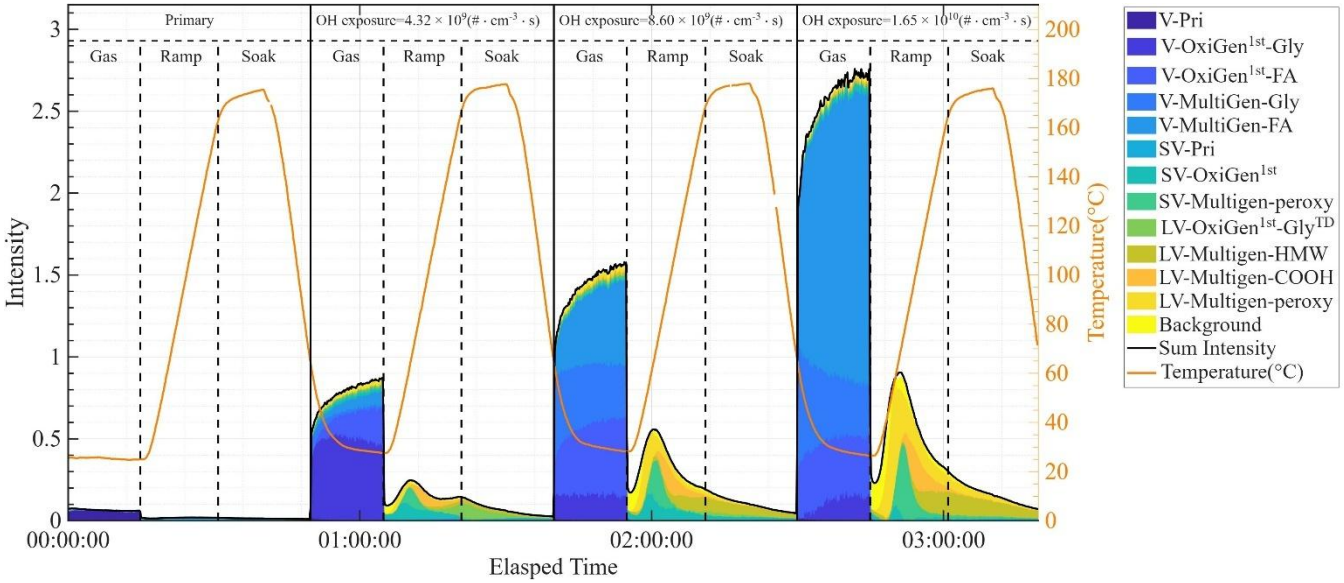

Figure 3 Factor time series of ME-2 PMF classification result with strengthen of OH exposure. Y-axis Intensity represents the sum of CIMS organic signal normalized to iodide ion other than formic acid.

3.4 Gas-particle partitioning of typical species.

Gas-particle partitioning is governed by both thermodynamic and kinetic processes. We compared characteristic time scales (τ) for gas-phase diffusion, surface desorption, and particle-phase diffusion with time scales apart from gas-particle partitioning served as reference, including particle coagulation, oxidation of cooking precursors (e.g., oleic acid), and residence in the Go:PAM. Detailed kinetic and thermodynamic estimation and parameterization methods are shown in **Section S5 of Supplement S1**, and the results are shown in **Figure 4**. Note that the kinetic estimations are based on Fickian diffusion and the fractional Stokes-Einstein relationship, which can undergo violation in secondary organic aerosol, especially for small molecules in in highly-oxidized aerosol(Marshall et al., 2016; Bedoya-Lora et al., 2019; Evoy et al., 2021; Mutneja and Karmakar, 2025). To ensure whether Fickian diffusion and fractional Stokes-Einstein relationship is adaptable in this system, Deborah number and Maxwell-Stefan diffusion coefficients are calculated and utilized to evaluated

their applicability, as described in **Section S5 of Supplement S1**. (Preston and Zuend, 2022). Results are shown in Figures **S6.42-6.44** of **Supplement S1**, indicating that deviations from the fractional Stokes-Einstein relationship and Fick's law are not expected to control the kinetics of the primary or secondary cooking aerosol under the investigated conditions, thus clarify the applicability of kinetic estimation utilized in this study(Pastore et al., 2021; Evoy et al., 2021; Preston, 2022).

Among gas-particle partitioning processes, particle-phase diffusion is the fastest modelled process in both primary and secondary aerosols across the investigated OH exposures, with τ values of approximately 10^{-2}–10^{0} s, substantially shorter than the 55 s residence time and the oxidation time scale of primary precursors, implying minor resistance of particle-phase diffusion on gas-particle partitioning under the modelled conditions. The reason of rapid particle-phase diffusion is liquid-like phase-state nature of primary and secondary organic aerosols regardless of viscosity parameterization methods, shown in **Figure S6.45-46**. Gas-phase diffusion time scale varied with both OH exposure and molecular weight. In primary aerosol, for most species with molar weight <150 g mol^{-1}, gas-phase diffusion time scale is over 10^{4} s, significantly slower(>3 order of magnitude) than any other processes in gas-particle partitioning and reference time scale, leading to more gas-phase-abundant partitioning compared to equilibrium state; for species with molar weight>150 g mol^{-1}, gas-phase diffusion time scale are comparable with coagulation time scale while still longer than other processes (about 1 order of magnitude). In the secondary aerosol, for some low-molecular-weight compounds with molar weight <120 g mol^{-1}, gas-phase diffusion time scale is still longer than retention time and oxidation time scale (about 1 order of magnitude); for other components, gas-phase diffusion time scale is shorter than retention time and oxidation time scale, with similar value to coagulation time scale (less than 1 order of magnitude). Surface-desorption time scales increase drastically with molecular weight: species with molecular weight >200 g mol^{-1} have desorption times longer than the residence time and account for approximately 10% of the total detected mass, whereas species with molecular weight >300 g mol^{-1} have desorption times longer than 1 h and account for approximately 5%. Surface desorption may therefore retain a limited fraction of high-molecular-weight compounds. In primary aerosols, large molecules with molar weight >250 g mol^{-1} would have both gas-phase diffusion and surface desorption time scale significantly longer than retention time, resulting in stable gas-particle partitioning characteristic only related to initial emission regardless of kinetic and thermodynamic property change. In secondary aerosols, $C_{>9}O_{>5}$ peroxides and auto oxidation products keeping long-chain fatty acid structures ($C_{16,18}O_{>4}$) would be confined to remain at aerosol phase due to kinetic limits in surface desorption process. Meanwhile, influence of surface desorption on semi- and intermediate- volatile components remains minor. Faster particle-phase diffusion and slightly slower gas-phase diffusion than coagulation is consistent with conclusions shown in Section 3.1, that the dominate SOA growth driving force is both condensation and coagulation. It should be noticed that, adsorption onto surface have already been considered in gas-phase time scale of gas-phase diffusion processes, utilizing the effective mass accommodation coefficient α_{eff} recommended by Shiraiwa et al.(Shiraiwa and Pöschl, 2021) accounting for particle-phase near-surface mass transport, rather than the pure surface accommodation coefficient α_s. Varying the surface mass accommodation coefficient from 1 to 0.01 by utilizing different α_s estimation methods would lead to significant variation of gas-phase diffusion time scale, while have minor effect on aerosol-phase diffusion time scale (**Figure 4 and Figures S6.48-6.49**), while ignoring near-surface

mass transfer would have similar or higher changes to gas-phase mass transfer time scale (**Figures S6.50**). This finding strengthens the suggestion on liquid-like, little-kinetic-limit aerosol phase of secondary cooking aerosol, indicate importance of surface processes (including surface accommodation and desorption) in gas-particle partitioning (Lbadaoui-Darvas et al., 2021; Knopf et al., 2024). We concluded a molecular-weight-dependent kinetic influence on gas-particle partitioning. Partitioning in primary aerosols consist of gas-phase favoured partitioning for species with molar mass<250 g mol^{-1} and emission-determined partitioning for species with molar mass>250 g mol^{-1}. Partitioning in primary aerosols consist of gas-phase favoured partitioning for small molecules with molar mass<120 g mol^{-1}, near-equilibrium partitioning for major components with molar mass between 120 g mol^{-1} and 220 g mol^{-1}, and particle-phase favoured partitioning for large molecules with molar mass>220 g mol^{-1}. Results show consistency with the minor changes on bulk composition because of possible major contribution of condensation onto particles rather than continuous oxidation the reason is that rate-determining step is gas-phase diffusion. Results are comparable to previous studies on primary and secondary cooking aerosol under the studied OH-exposure range (<10^{10} molecules cm^{-3} s)(Takhar et al., 2021; Masoud et al., 2022; Hou et al., 2025; Liu et al., 2025).

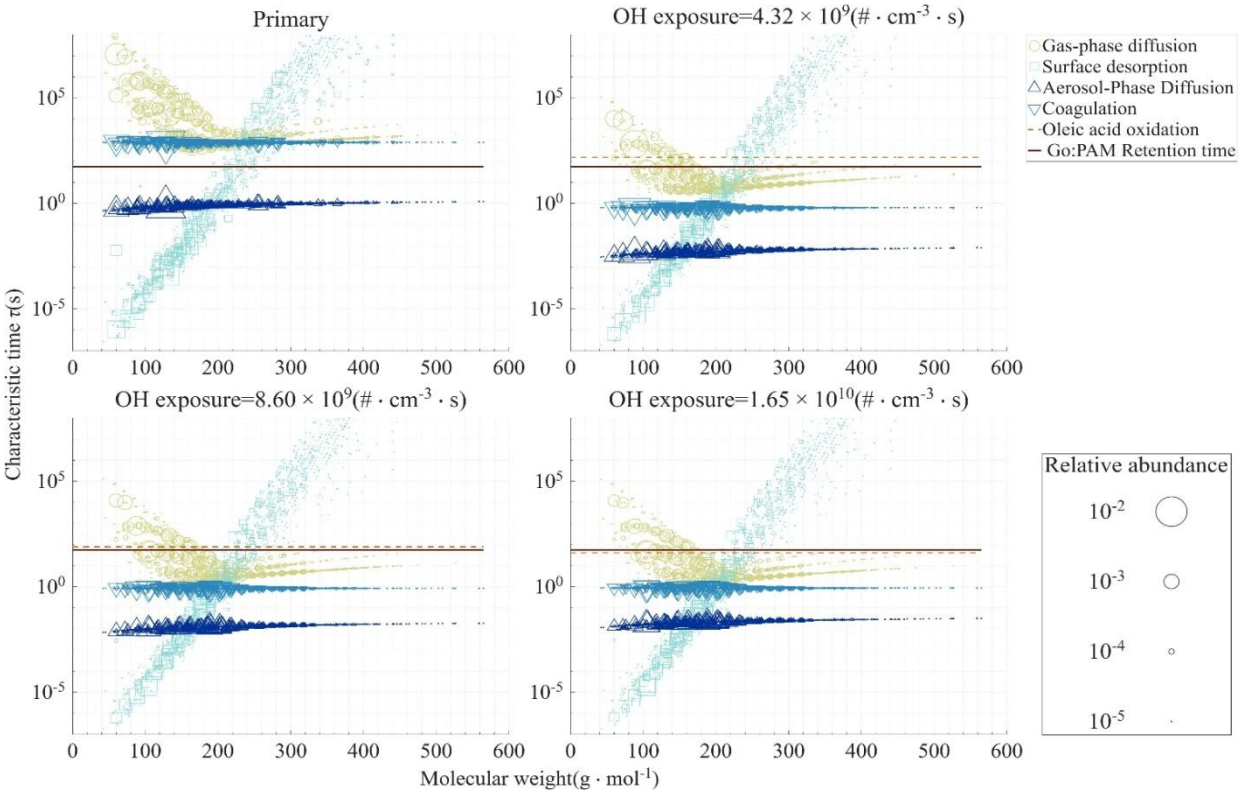

Figure 4 The characteristic time scale of FIGAERO-CIMS detected species in various kinetic transport processes of gas-particle partitioning with enhancement of OH exposure. Markers show time scale of gas-phase diffusion(circle), surface desorption(square), aerosol-phase diffusion(triangle), coagulation (reverse triangle). Lines shows reference time scale, including retention time(solid) and oleic acid oxidation(dashed). Marker size represents relative abundance of species. Surface mass accommodation coefficients are estimated based on parametrization method 1 shown in Section S5.

Here we compared estimated and measured volatilities of species in cooking aerosol after accounting for activity coefficients and the Kelvin effect (see **Figure 5**). Adsorption equilibrium partitioning theory are utilized because of liquid-like nature of primary and secondary aerosols. Liquid-liquid phase separation (LLPS) was also considered and was not predicted to occur under the modeled conditions because none of the species had a particle-phase activity near or above unity (**Figure S6.41)**. Volatility derived from the FIGAERO particle-phase fraction and thermogram peak temperature are generally low and distributed more narrowly than the theoretical estimates. Specifically, based on FIGAERO measurements, the equilibrium theory performed fine on estimation S/IVOCs with $\log_{10}C^*$ in $\mu g \cdot m^{-3}$ within range of 3~5, corresponding to compounds with molecular weight 120-220 in secondary organic aerosols. However, it overestimates the volatility of the other highly abundant SVOC to IVOC species by 1-3 order of magnitude, while underestimate the volatility of LVOCs. These gaps are higher for IVOC and LVOC, while closer at the boundary of SVOC to IVOC. Possible explanations on discrepancies between measurement and parametrization include instrumentation limits in FIGAERO measurements, such as hindered evaporation and desorption caused by the FIGAERO filter microstructure (Ylisirniö et al., 2021; Ylisirniö et al., 2025). Another possible cause might be aerosol microstructure influence of functionalized auto-oxidation product or uncertainty on activity coefficients(Wang et al., 2026; Zhang et al., 2024; Chen et al., 2025). Sensitivity test has been done by adding long-chain-fatty-acid related species into measurement result to observe the difference of thermodynamics and kinetics **(Figures S6.53-S6.54)**, showing potential underestimation would not interfere thermodynamic and kinetic estimations, indicating minor effect of fatty-acid-related instrument sensitivity. Even so, large molecules may still subject to additional mass transfer limitations, including surface effects, which may be an optional cause of phenomenon that detected large molecules bias toward gas phase. (Zaveri et al., 2018; Masoud et al., 2022; Schervish and Shiraiwa, 2023).

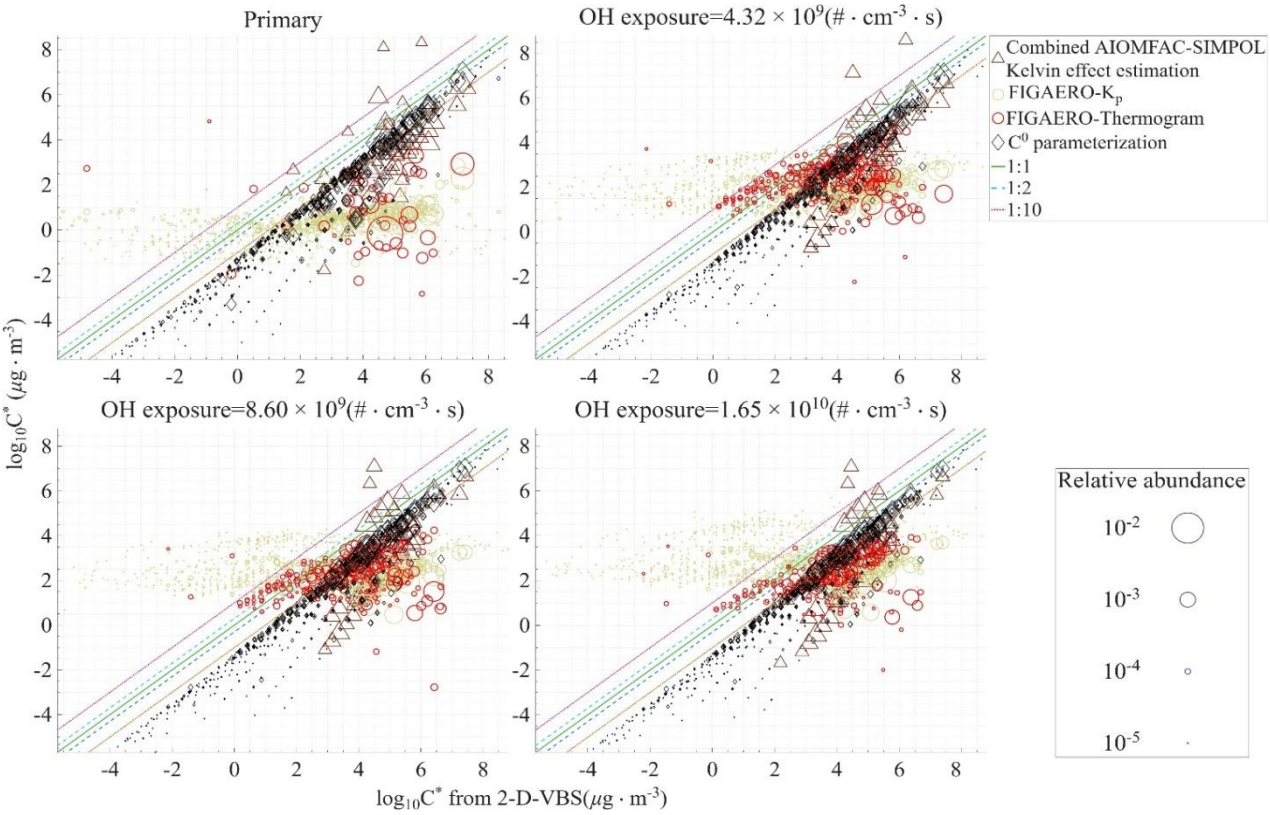

Figure 5 The characteristic effective saturated concentration C^* of FIGAERO-CIMS detected species utilizing different estimation methods with enhancement of OH exposure. Markers show combined AIOMFAC-SIMPOL vapor-pressure and activity coefficient estimation methods accounting for kelvin effect (triangle), K_p from FIGAERO measurements (yellow circle), T_{max} from FIGAERO thermograms (red circle), C^* parametrization(West et al., 2023) (reverse triangle). Lines shows 1:1,1:2 and 1:10 position. Marker size represents relative abundance of species.

To achieve more comprehensive and detailed knowledge on thermodynamic properties and influence on gas-particle partitioning, we select typical species from ME-2 PMF factors using ordinal analysis method. Most abundant species in each factor representing different oxidative state, volatility and precursor type are shown in Tables **S6.1-6.12** in Supplement S1. We further select the most representative species and list them in **Table 2.** Among species in **Table 2**, highly-volatile low-molecular-weight compounds, such as formic acid and acetic acid, are typically volatile organic aerosol species. The abundance of these volatile species detected in "aerosol phase" are probably resulting from thermal decomposition. We would then mainly focus on semi-volatile and low-volatile species with considerable gas-particle partitioning influence on SOA formation and evolution. These key species, including primary species related to cooking emissions(Reyes-Villegas et al., 2018), intermediate oxidative state species related to first-generation oxidation or thermal oxidation(Takhar et al., 2022), and multi-generation termination oxidation products(Masoud et al., 2022; Brown et al., 2021; Takhar et al., 2021), are listed in **Table 2**.

Table 2 Classified typical species at various oxidative state

Oxidative state	Volatility	Formula	Possible species	p^0(Pa,25 ℃)
Primary	Semi-volatile	$C_3H_8O_3$	Glycerol	2.24×10^{-2}
		$C_{16}H_{32}O_2$	Palmitic acid	2.67×10^{-5}
		$C_{18}H_{34}O_2$	Oleic acid	1.12×10^{-4}
First-generation	Semi-volatile	$C_3H_4O_3$	Pyruvic acid	1.72×10^{2}
		$C_7H_{12}O_3$	-	1.18×10^{0}
		$C_{10}H_{16}O_3$	-	1.09×10^{-1}
	Low-volatile	$C_{16}H_{32}O_3$	-	6.96×10^{-6}
Multi-generations	Semi-volatile	$C_4H_6O_4$	Succinic acid	1.04×10^{-3}
		$C_6H_{10}O_4$	Adipic acid	5.4×10^{-4}
		$C_9H_{16}O_4$	Azelaic acid	4.74×10^{-5}
	Low-volatile	$C_{10}H_{18}O_5$	-	4.02×10^{-5}
		$C_{18}H_{32}O_6$	-	1.39×10^{-8}

Figure 6 compares measured and equilibrium-predicted K_p values for the representative species listed in **Table 2** across the investigated OH exposures. The panels show primary species, first-generation oxidation products, and multigenerational oxidation products, respectively. The subplot legends indicate the oxidation degree of each component, where dashed lines represent estimated values and solid lines denote experimental values. Specifically, among primary emission components, the gas-particle partitioning of typical species deviate toward aerosol phase, due to limitations on gas-particle partitioning refined to initial emission compositions mentioned before. With oxidation proceeds leading to SOA formation, the partitioning coefficient of primary components decreases significantly closer to theoretical values, indicating SOA formation would relieve the gas-phase diffusion limit by increasing surface area of aerosols, and thus consumption of primary components pushes the gas-particle partitioning toward equilibrium especially for oxidation products at S/IVOC range. Among first-generation oxidation products, components with $C_{\geq5}$ primarily originating from fatty acid cleavage are predominate, while a minority of $C_{\leqslant4}$ components derive from glycerol oxidation existed. The theoretical K_p values for $C_{\geq5}$ first-generation oxidation products generated via fragmentation reactions are markable lower than FIGAERO-measured values, indicating a substantial deviation from equilibrium in their gas-particle partitioning. Functionalized multi-generation oxidation products from scissoring of long-chain fatty acids including $C_{16}H_{32}O_3$, $C_{18}H_{32}O_6$ and exhibit lesser deviation from estimated, possibly due to its structure similarity with aerosol bulk composition; However, large molecule oxidation products ($C_{\geq12}O_{\geq5}$, e.g., $C_{18}H_{32}O_6$) demonstrate significant deviations. Estimates based on equilibrium partitioning suggest that these components should only occupy a minimal fraction in the gas phase; however, measurement results in substantial gas-phase presence, consistent with general results shown in **Figure 5.**

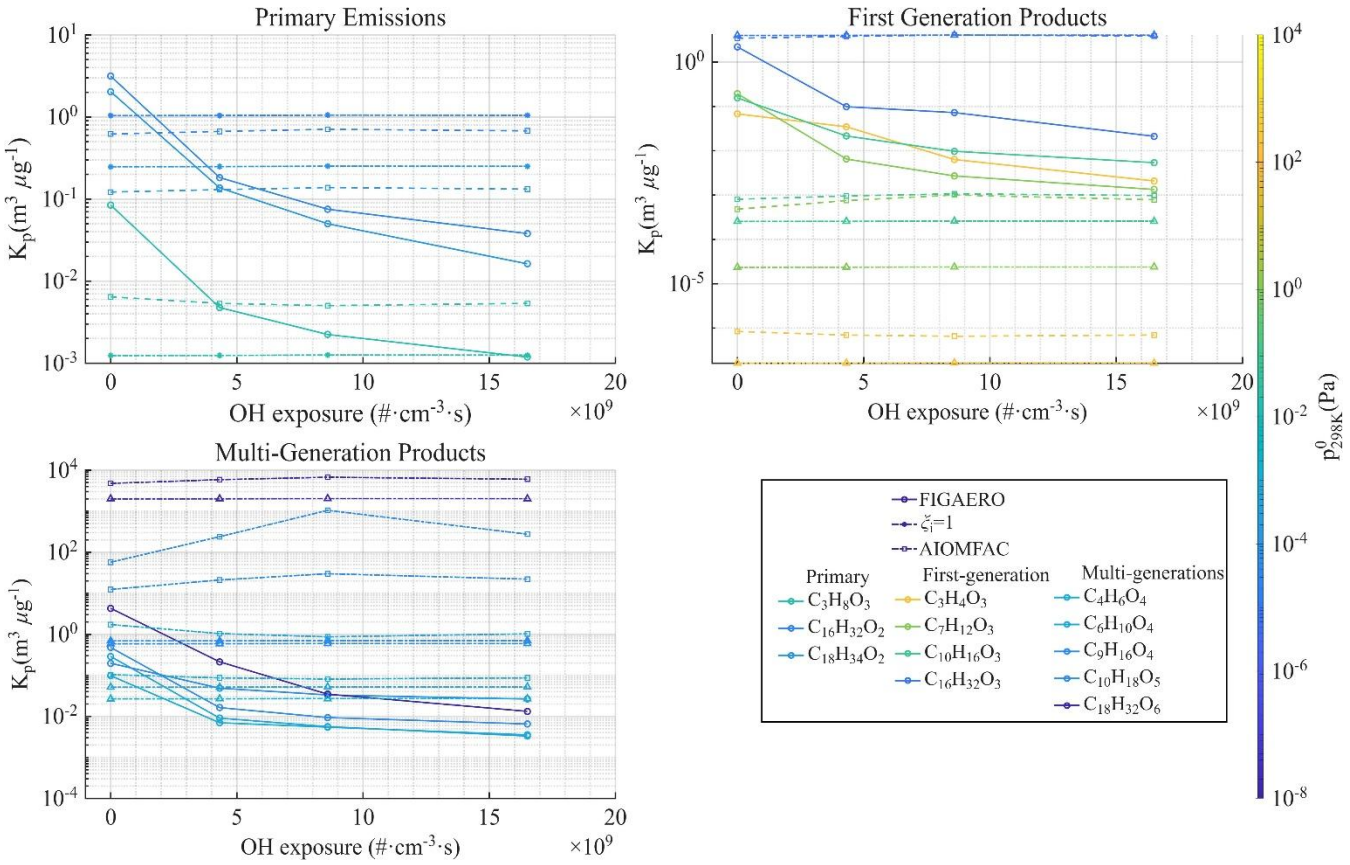

Figure 6 measurement and estimated partitioning coefficient (K_p) evolution of typical species of (a) primary emission (b) first generation products (c) multi-generation oxidation products

We concluded that among key species in primary and secondary organic aerosols, gas-particle partitioning of low-molecular-weight, moderately-oxidized species ($C_{3-8}O_{3-4}$) and highly oxidized large species ($C_{\geq12}O_{\geq5}$) are biased from the ideal equilibrium estimates, while medium-molecular-weight components ($C_{5\text{-}10}O_{4\text{-}5}$, $\log_{10}C^*$ in $\mu g \cdot m^{-3}$ 3-5) shows near-equilibrium partitioning characteristics. The theoretical approach overestimates K_p of $C_{3-8}O_{3-4}$ species and underestimates K_p of $C_{\geq12}O_{\geq5}$ species. As thermodynamic and kinetic estimation results revealed, deviations from equilibrium state should not be assigned to a single process. Non-ideal thermodynamics, including composition-dependent activity coefficients, can alter partitioning relative to an ideal organic solution. While a liquid-like aerosol phase would not cause aerosol-phase diffusion limit or forming viscous shells , gas-phase diffusion limitation in primary aerosols and surface mass transfer limitations in cooking aerosols would result in bias from equilibrium state, especially for small and large molecules. . In addition, uncertainties in pure-component vapor pressures, activity coefficients, FIGAERO quantification, filter-mediated desorption, and thermal decomposition or rearrangement can both affect the comparison. We therefore confirmed the applicability of equilibrium gas-particle partitioning in estimating typical cooking-related secondary species with $C_{5\text{-}10}O_{4\text{-}5}$, $\log_{10}C^*$ between 3-5 in $\mu g \cdot m^{-3}$, and interpret the compound-class bias from equilibrium as a combined thermodynamic, kinetic, and

measurement-model discrepancy rather than as direct evidence of particle-phase (Shiraiwa et al., 2012; Zhang et al., 2012; Zaveri et al., 2018). As an intrinsic property of FIGAERO-CIMS instrumentation, thermal desorption related measurement uncertainties, including thermal decomposition, may also contribute to the observed deviations(Mehra et al., 2020; Tikkanen et al., 2020; Masoud et al., 2022). The gap remains the crucial challenge in gas-particle partitioning studies, here we descript the phenomenon in a rigorous way.

4. Conclusion

This study presents a comprehensive investigation into the atmospheric evolution of cooking-derived organic aerosols, integrating advanced analytical techniques to unravel complex gas-particle dynamics. Using a Go:PAM oxidation flow reactor together with FIGAERO-I-CIMS measurements, we characterized changes in molecular composition, volatility, and gas-particle partitioning across the investigated OH exposures. A key innovation lies in the combined application of high-resolution mass spectrometry with a two-dimensional volatility basis set (2-D VBS) framework, enabling a mechanistic understanding of composition-dependent partitioning behavior.

Under typical atmospheric conditions, primary cooking emissions rapidly generated substantial quantities of fine particles (~10 nm) within two hours, followed by the formation of higher concentrations of 30–50 nm secondary aerosols over 0.5-1 days. Notably, oxidation products predominantly occupied the semi-volatile and intermediate-volatility organic compounds (S/IVOCs) range in the 2-D VBS, systematically migrating toward the SVOC region as oxidation progressed, while molecular weight and oxidation degree remained relatively stable. Leveraging positive matrix factorization (PMF), we systematically classified compounds by oxidation degree and volatility, identifying representative markers across evolution stages: gaseous glycerol and particulate long-chain fatty acids in primary emissions; medium-weight carbonyl acids (e.g., $C_5H_{10}O_3$, $C_7H_{12}O_3$) as intermediate products, and multi-generation oxidation products including dicarboxylic acids (e.g., $C_9H_{16}O_4$) and HOM-like compounds (e.g., $C_{18}H_{32}O_{5-6}$) as mature products. Of particular importance are highly oxidized small organic acids ($\leq C_3$) and multi-generation products in the C_7-C_{10} range with moderate volatility and high oxidation state. A central finding concerns the thermodynamics and kinetics gas-particle partitioning observed across different compound classes. Observation shows that fragmentation-derived functionalized multi-generation oxidation products exhibits near equilibrium state, and identified significant kinetic limitations for first-generation oxidation products ($C_{3-8}O_{3-4}$) and large non-cleavage products ($>C_{14}O_5$), which exhibited significant deviations from equilibrium. Based on comprehensive estimation and parametrization of kinetic and thermodynamic processes, we concluded that the secondary cooking aerosol in this study are near equilibrium state for typical secondary S/IVOCs that are predominant in this study, while partitioning in primary aerosols, and for low-molecular-weight and high-molecular-weight species in secondary are constrained Surface processes account for most gas-particle partitioning kinetic limits for most non-equilibrium-partitioning compounds . Thermodynamic analysis unravels gap between theory and measurements especially for small and large molecules, requiring further instrumentation and theory development. The mechanistic insight into partitioning dynamics represents a significant

advance in understanding the atmospheric behavior of cooking emissions, given clear evidence in a liquid-like and weak kinetic limited aerosol phase and a surface-mass-transfer limited gas-particle partitioning scheme for cooking and even other anthropogenic and natural emissions with OH radical as oxidant and long-chain-hydrocarbon-like species as precursors. Our results provide a scientific foundation for refining emission inventories and air quality models, ultimately contributing to improved exposure assessment and mitigation strategies for urban and indoor environments.

Code, data, or code and data availability

Data will be available upon request.

Supplement link

Supplementary material is available in the online version of this article.

Author contributions

RS: Conceptualization, Experimentation, Data curation, Formal analysis, Methodology, Visualization, Validation, Writing (original draft preparation).
SG: Conceptualization, Formal analysis, Funding acquisition, Project administration, Supervision.
HW: Experimentation, Data curation, Formal analysis, Methodology, Validation, Supervision.
YY: Experimentation, Data curation, Formal analysis, Methodology, Validation, Supervision.
ZW: Validation, Supervision, Writing (review and editing).
RT: Experimentation, Data curation, Methodology, Validation.
WZ: Experimentation, Methodology, Validation.
ZC: Experimentation, Validation.
SC: Experimentation, Resources, Validation.
ZW: Funding acquisition, Supervision.
SL, YC: Funding acquisition and Resources, providing custom-designed cooking-emission laboratory.
MH: Funding acquisition, Supervision.

Competing interests

Authors declare no known competing interests.

Acknowledgements

BThis research was supported by the National Key R&D Program of China (2022YFC3701000, Task 2), National Natural Science Foundation of China-Creative Research Group Fund (22221004), special fund of State Key Laboratory of Regional Environment and Sustainability (26Y01RESPKU).

References

Abdullahi, K. L., Delgado-Saborit, J. M., and Harrison, R. M.: Emissions and indoor concentrations of particulate matter and its specific chemical components from cooking: A review, Atmospheric Environment, 71, 260-294, 10.1016/j.atmosenv.2013.01.061, 2013.

Aladedunye, F.: Toxic contaminants of thermo-oxidatively processed edible oils/fats, Lipid Technol., 28, 117-121, 10.1002/lite.201600032, 2016.

Atkinson, R., Baulch, D. L., Cox, R. A., Crowley, J. N., Hampson, R. F., Hynes, R. G., Jenkin, M. E., Rossi, M. J., Troe, J., and Subcommittee, I.: Evaluated kinetic and photochemical data for atmospheric chemistry: Volume II – gas phase reactions of organic species, Atmos. Chem. Phys., 6, 3625-4055, 10.5194/acp-6-3625-2006, 2006.

Bandowe, B. A. M., Lui, K. H., Jones, T., BeruBe, K., Adams, R., Niu, X., Wei, C., Cao, J. J., Lee, S. C., Chuang, H. C., and Ho, K. F.: The chemical composition and toxicological effects of fine particulate matter (PM(2.5)) emitted from different cooking styles, Environ Pollut, 288, 117754, 10.1016/j.envpol.2021.117754, 2021.

Bannan, T. J., Le Breton, M., Priestley, M., Worrall, S. D., Bacak, A., Marsden, N. A., Mehra, A., Hammes, J., Hallquist, M., Alfarra, M. R., Krieger, U. K., Reid, J. P., Jayne, J., Robinson, W., McFiggans, G., Coe, H., Percival, C. J., and Topping, D.: A method for extracting calibrated volatility information from the FIGAERO-HR-ToF-CIMS and its experimental application, Atmospheric Measurement Techniques, 12, 1429-1439, 10.5194/amt-12-1429-2019, 2019.

Bedoya-Lora, F. E., Echeverria, F., and Calderon, J. A.: Effectiveness of non-Fickian diffusion model on the water uptake determination of different organic coatings, Progress in Organic Coatings, 136, 10.1016/j.porgcoat.2019.06.052, 2019.

Bonetti, R. and Parker, W. O.: Insights into Polymerization of Vegetable Oil: Oligomerization of Oleic Acid, JAOCS J Am Oil Chem Soc, 96, 1181-1184, 10.1002/aocs.12274, 2019.

Brown, W. L., Day, D. A., Stark, H., Pagonis, D., Krechmer, J. E., Liu, X., Price, D. J., Katz, E. F., DeCarlo, P. F., Masoud, C. G., Wang, D. S., Hildebrandt Ruiz, L., Arata, C., Lunderberg, D. M., Goldstein, A. H., Farmer, D. K., Vance, M. E., and Jimenez, J. L.: Real-time organic aerosol chemical speciation in the indoor environment using extractive electrospray ionization mass spectrometry, Indoor Air, 31, 141-155, 10.1111/ina.12721, 2021.

Buchholz, A., Ylisirniö, A., Huang, W., Mohr, C., Canagaratna, M., Worsnop, D. R., Schobesberger, S., and Virtanen, A.: Deconvolution of FIGAERO-CIMS thermal desorption profiles using positive matrix factorisation to identify chemical and physical processes during particle evaporation, Atmospheric Chemistry and Physics, 20, 7693-7716, 10.5194/acp-20-7693-2020, 2020a.

Buchholz, A., Ylisirniö, A., Huang, W., Mohr, C., Canagaratna, M., Worsnop, D. R., Schobesberger, S., and Virtanen, A.: Deconvolution of FIGAERO–CIMS thermal desorption profiles using positive matrix factorisation to identify chemical and physical processes during particle evaporation, Atmos. Chem. Phys., 20, 7693-7716, 10.5194/acp-20-7693-2020, 2020b.

Cai, X. and Griffin, R. J.: Modeling the formation of secondary organic aerosol in coastal areas: Role of the sea-salt aerosol organic layer, Journal of Geophysical Research: Atmospheres, 108, 10.1029/2002JD003053, 2003.

Canonaco, F., Crippa, M., Slowik, J. G., Baltensperger, U., and Prévôt, A. S. H.: SoFi, an IGOR-based interface for the efficient use of the generalized multilinear engine (ME-2) for the source apportionment: ME-2 application to aerosol mass spectrometer data, Atmospheric Measurement Techniques, 6, 3649-3661, 10.5194/amt-6-3649-2013, 2013.

Chandramouli, B., Jang, M., and Kamens, R. M.: Gas–particle partitioning of semi-volatile organics on organic aerosols using a predictive activity coefficient model: analysis of the effects of parameter choices on model performance, Atmospheric Environment, 37, 853-864, 10.1016/s1352-2310(02)00931-7, 2003.

Chen, Y., Xia, M., Zheng, P., Li, Y., Zou, Z., Tong, S., Li, K., Feng, X., Hui, L., Yuan, Q., Li, J., Yu, J. Z., Lee, S., Wang, T., and Wang, Z.: Complex gas-particle partitioning of nitro-phenolic compounds: field-based insights and determination of apparent activity coefficient, npj Climate and Atmospheric Science, 8, 10.1038/s41612-025-01156-z, 2025.
Chiaia, V., Micalizzi, G., Donnarumma, D., Irto, A., Bretti, C., Venuti, M., Lando, G., Mondello, L., and Cardiano, P.: Study of oxidation products in aged olive oils by GC and HPLC techniques coupled to mass spectrometry to discriminate olive oil lipid substances in archaeological artifacts from ancient Taormina (Italy), Journal of Chromatography A, 1731, 10.1016/j.chroma.2024.465154, 2024.
Chuang, W. K. and Donahue, N. M.: A two-dimensional volatility basis set – Part 3: Prognostic modeling and NOx dependence, Atmospheric Chemistry and Physics, 16, 123-134, 10.5194/acp-16-123-2016, 2016.
Donahue, N. M., Epstein, S. A., Pandis, S. N., and Robinson, A. L.: A two-dimensional volatility basis set: 1. organic-aerosol mixing thermodynamics, Atmospheric Chemistry and Physics, 11, 3303-3318, 10.5194/acp-11-3303-2011, 2011.
Donahue, N. M., Kroll, J. H., Pandis, S. N., and Robinson, A. L.: A two-dimensional volatility basis set – Part 2: Diagnostics of organic-aerosol evolution, Atmospheric Chemistry and Physics, 12, 615-634, 10.5194/acp-12-615-2012, 2012.
Du, Y., Che, H., Bao, Z., Liu, Y., Li, Q., Hu, M., Zhou, J., Zhang, S., Yao, X., Shi, Q., Chen, C., Han, Y., Meng, L., Long, X., Qi, X., He, C., and Chen, Y.: Evolution of atmospheric high-molecular-weight Organonitrates (HMW ONs) in urban Yangtze River Delta (YRD), China, npj Climate and Atmospheric Science, 8, 10.1038/s41612-025-00928-x, 2025.
Evoy, E., Kiland, K. J., Huang, Y., Schnitzler, E. G., MacLean, A. M., Kamal, S., Abbatt, J. P. D., and Bertram, A. K.: Diffusion Coefficients and Mixing Times of Organic Molecules in β-Caryophyllene Secondary Organic Aerosol (SOA) and Biomass Burning Organic Aerosol (BBOA), ACS Earth and Space Chemistry, 5, 3268-3278, 10.1021/acsearthspacechem.1c00317, 2021.
Farmer, D. K., Vance, M. E., Abbatt, J. P. D., Abeleira, A., Alves, M. R., Arata, C., Boedicker, E., Bourne, S., Cardoso-Saldana, F., Corsi, R., DeCarlo, P. F., Goldstein, A. H., Grassian, V. H., Hildebrandt Ruiz, L., Jimenez, J. L., Kahan, T. F., Katz, E. F., Mattila, J. M., Nazaroff, W. W., Novoselac, A., O'Brien, R. E., Or, V. W., Patel, S., Sankhyan, S., Stevens, P. S., Tian, Y., Wade, M., Wang, C., Zhou, S., and Zhou, Y.: Overview of HOMEChem: House Observations of Microbial and Environmental Chemistry, Environ Sci Process Impacts, 21, 1280-1300, 10.1039/c9em00228f, 2019.
Frankel, E. N., Neff, W. E., and Selke, E.: Analysis of autoxidized fats by gas chromatography-mass spectrometry: VIII. Volatile thermal decomposition products of hydroperoxy cyclic peroxides, Lipids, 18, 353-357, 10.1007/BF02537231, 1983.
Grebenteuch, S., Kroh, L. W., Drusch, S., and Rohn, S.: Formation of secondary and tertiary volatile compounds resulting from the lipid oxidation of rapeseed oil, Foods, 10, 10.3390/foods10102417, 2021.
Guo, S., Hu, M., Peng, J., Wu, Z., Zamora, M. L., Shang, D., Du, Z., Zheng, J., Fang, X., Tang, R., Wu, Y., Zeng, L., Shuai, S., Zhang, W., Wang, Y., Ji, Y., Li, Y., Zhang, A. L., Wang, W., Zhang, F., Zhao, J., Gong, X., Wang, C., Molina, M. J., and Zhang, R.: Remarkable nucleation and growth of ultrafine particles from vehicular exhaust, P Natl Acad Sci USA, 117, 3427-3432, 10.1073/pnas.1916366117, 2020.
Guo, Z., Chen, X., Wu, D., Huo, Y., Cheng, A., Liu, Y., Li, Q., and Chen, J.: Higher Toxicity of Gaseous Organics Relative to Particulate Matters Emitted from Typical Cooking Processes, Environmental Science & Technology, 57, 17022-17031, 10.1021/acs.est.3c05425, 2023.
Hallquist, M., Wenger, J. C., Baltensperger, U., Rudich, Y., Simpson, D., Claeys, M., Dommen, J., Donahue, N. M., George, C., Goldstein, A. H., Hamilton, J. F., Herrmann, H., Hoffmann, T., Iinuma, Y., Jang, M., Jenkin, M. E., Jimenez, J. L., Kiendler-Scharr, A., Maenhaut, W., McFiggans, G., Mentel, T. F., Monod, A., Prévôt, A. S. H., Seinfeld, J. H., Surratt, J. D., Szmigielski, R., and Wildt, J.: The formation, properties and impact of secondary organic aerosol: current and emerging issues, Atmos. Chem. Phys., 9, 5155-5236, 10.5194/acp-9-5155-2009, 2009.
Hashimoto, S., Takazawa, Y., Ieda, T., Omagari, R., Nakajima, D., Nakamura, S., and Suzuki, N.: Application of rapid air sampling and non-targeted analysis using thermal desorption comprehensive two-dimensional gas chromatography/time-of-flight mass spectrometry to accidental fire, Chemosphere, 303, 10.1016/j.chemosphere.2022.135021, 2022.
He, L.-Y., Hu, M., Huang, X.-F., Yu, B.-D., Zhang, Y.-H., and Liu, D.-Q.: Measurement of emissions of fine particulate organic matter from Chinese cooking, Atmospheric Environment, 38, 6557-6564, 10.1016/j.atmosenv.2004.08.034, 2004.
Hou, S., Liu, W., and Kuwata, M.: Fresh Cooking Organic Aerosol Particles Exist as Liquid in Most Urban Temperature Range, Journal of Geophysical Research: Atmospheres, 130, 10.1029/2025JD043825, 2025.
Iyer, S., Lopez-Hilfiker, F., Lee, B. H., Thornton, J. A., and Kurten, T.: Modeling the Detection of Organic and Inorganic Compounds Using Iodide-Based Chemical Ionization, J Phys Chem A, 120, 576-587, 10.1021/acs.jpca.5b09837, 2016.

Kawada, T., Krishnamurthy, R. G., Mookherjee, B. D., and Chang, S. S.: Chemical reactions involved in the deep fat frying of foods. II. Identification of acidic volatile decomposition products of corn oil, Journal of the American Oil Chemists' Society, 44, 131-135, 10.1007/BF02558172, 1967.

Knopf, D. A., Ammann, M., Berkemeier, T., Pöschl, U., and Shiraiwa, M.: Desorption lifetimes and activation energies influencing gas–surface interactions and multiphase chemical kinetics, Atmospheric Chemistry and Physics, 24, 3445-3528, 10.5194/acp-24-3445-2024, 2024.

Kong, X., Salvador, C. M., Carlsson, S., Pathak, R., Davidsson, K. O., Le Breton, M., Gaita, S. M., Mitra, K., Hallquist, A. M., Hallquist, M., and Pettersson, J. B. C.: Molecular characterization and optical properties of primary emissions from a residential wood burning boiler, Sci Total Environ, 754, 142143, 10.1016/j.scitotenv.2020.142143, 2021.

Kristensen, K., Lunderberg, D. M., Liu, Y., Misztal, P. K., Tian, Y., Arata, C., Nazaroff, W. W., and Goldstein, A. H.: Gas–Particle Partitioning of Semivolatile Organic Compounds in a Residence: Influence of Particles from Candles, Cooking, and Outdoors, Environmental Science & Technology, 57, 3260-3269, 10.1021/acs.est.2c07172, 2023.

Lbadaoui-Darvas, M., Takahama, S., and Nenes, A.: Molecular-scale description of interfacial mass transfer in phase-separated aqueous secondary organic aerosol, Atmospheric Chemistry and Physics, 21, 17687-17714, 10.5194/acp-21-17687-2021, 2021.

Le Breton, M., Psichoudaki, M., Hallquist, M., Watne, Å. K., Lutz, A., and Hallquist, Å. M.: Application of a FIGAERO ToF CIMS for on-line characterization of real-world fresh and aged particle emissions from buses, Aerosol Science and Technology, 53, 244-259, 10.1080/02786826.2019.1566592, 2019.

Lee, B. H., Lopez-Hilfiker, F. D., Mohr, C., Kurten, T., Worsnop, D. R., and Thornton, J. A.: An Iodide-Adduct High-Resolution Time-of-Flight Chemical-Ionization Mass Spectrometer: Application to Atmospheric Inorganic and Organic Compounds, Environmental Science & Technology, 48, 6309-6317, 10.1021/es500362a, 2014.

Li, Y.-C., Shu, M., Ho, S. S. H., Wang, C., Cao, J.-J., Wang, G.-H., Wang, X.-X., Wang, K., and Zhao, X.-Q.: Characteristics of PM2.5 emitted from different cooking activities in China, Atmospheric Research, 166, 83-91, 10.1016/j.atmosres.2015.06.010, 2015.

Li, Y., Pöschl, U., and Shiraiwa, M.: Molecular corridors and parameterizations of volatility in the chemical evolution of organic aerosols, Atmospheric Chemistry and Physics, 16, 3327-3344, 10.5194/acp-16-3327-2016, 2016.

Lin, C., Huang, R. J., Duan, J., Zhong, H., and Xu, W.: Polycyclic aromatic hydrocarbons from cooking emissions, Sci Total Environ, 151700, 10.1016/j.scitotenv.2021.151700, 2021.

Liu, W., He, L., Li, Y., Li, P., Chen, S., Chen, J., Liu, Y., and Kuwata, M.: Prolonged Atmospheric Chemical Lifetime of Unsaturated Fatty Acids From Cooking Sources Observed in Beijing During Wintertime, Journal of Geophysical Research: Atmospheres, 130, 10.1029/2025JD044172, 2025.

Liu, W., Zhou, L., Yuan, W., Ruan, L., Wang, X., Guo, Y., Xie, Z., Liu, Q., and Wang, C.: Tracking indoor volatile organic compounds with online mass spectrometry, TrAC Trends Anal. Chem., 171, 10.1016/j.trac.2023.117514, 2024.

Lopez-Hilfiker, F. D., Pospisilova, V., Huang, W., Kalberer, M., Mohr, C., Stefenelli, G., Thornton, J. A., Baltensperger, U., Prevot, A. S. H., and Slowik, J. G.: An extractive electrospray ionization time-of-flight mass spectrometer (EESI-TOF) for online measurement of atmospheric aerosol particles, Atmospheric Measurement Techniques, 12, 4867-4886, 10.5194/amt-12-4867-2019, 2019.

Lopez-Hilfiker, F. D., Mohr, C., Ehn, M., Rubach, F., Kleist, E., Wildt, J., Mentel, T. F., Lutz, A., Hallquist, M., Worsnop, D., and Thornton, J. A.: A novel method for online analysis of gas and particle composition: description and evaluation of a Filter Inlet for Gases and AEROsols (FIGAERO), Atmospheric Measurement Techniques, 7, 983-1001, 10.5194/amt-7-983-2014, 2014.

Lopez-Hilfiker, F. D., Mohr, C., D'Ambro, E. L., Lutz, A., Riedel, T. P., Gaston, C. J., Iyer, S., Zhang, Z., Gold, A., Surratt, J. D., Lee, B. H., Kurten, T., Hu, W. W., Jimenez, J., Hallquist, M., and Thornton, J. A.: Molecular Composition and Volatility of Organic Aerosol in the Southeastern U.S.: Implications for IEPOX Derived SOA, Environ Sci Technol, 50, 2200-2209, 10.1021/acs.est.5b04769, 2016.

Lopez-Pedrajas, S., Estevez, R., Schnee, J., Gaigneaux, E. M., Luna, D., and Bautista, F. M.: Study of the gas-phase glycerol oxidehydration on systems based on transition metals (Co, Fe, V) and aluminium phosphate, Molecular Catalysis, 455, 68-77, 10.1016/j.mcat.2018.05.020, 2018.

Lu, L., Ng, V. Y. Z., Tan, M. Z. H., Kasthuriarachchi, N. Y., Rivellini, L.-H., Tan, Y. Q., Ang, L., Viera, M., Bay, B. H., Seow, W. J., and Lee, A. K. Y.: Particle-bound reactive oxygen species in cooking emissions: Aging effects and cytotoxicity, Atmospheric Environment, 319, 10.1016/j.atmosenv.2023.120309, 2024.

Luo, Z., Zang, H., Li, Z., Li, C., and Zhao, Y.: Species-specific effect of particle viscosity and particle-phase reactions on the formation of secondary organic aerosol, Science of The Total Environment, 950, 10.1016/j.scitotenv.2024.175207, 2024.

Marshall, F. H., Miles, R. E. H., Song, Y. C., Ohm, P. B., Power, R. M., Reid, J. P., and Dutcher, C. S.: Diffusion and reactivity in ultraviscous aerosol and the correlation with particle viscosity, Chem Sci, 7, 1298-1308, 10.1039/c5sc03223g, 2016.

Martins, G. B. C., Mello, V. M., and Suarez, P. A. Z.: Thermal processes in fats and oils, Rev. Virtual Quim., 5, 16-25, 10.5935/1984-6835.20130003, 2013.

Masoud, C. G., Li, Y., Wang, D. S., Katz, E. F., DeCarlo, P. F., Farmer, D. K., Vance, M. E., Shiraiwa, M., and Hildebrandt Ruiz, L.: Molecular composition and gas-particle partitioning of indoor cooking aerosol: Insights from a FIGAERO-CIMS and kinetic aerosol modeling, Aerosol Science and Technology, 56, 1156-1173, 10.1080/02786826.2022.2133593, 2022.

Mehra, A., Krechmer, J. E., Lambe, A., Sarkar, C., Williams, L., Khalaj, F., Guenther, A., Jayne, J., Coe, H., and Worsnop, D.: Oligomer and highly oxygenated organic molecule formation from oxidation of oxygenated monoterpenes emitted by California sage plants, Atmospheric Chemistry and Physics, 20, 10953-10965, 10.5194/acp-20-10953-2020, 2020.

Milsom, A., Squires, A. M., Boswell, J. A., Terrill, N. J., Ward, A. D., and Pfrang, C.: An organic crystalline state in ageing atmospheric aerosol proxies: spatially resolved structural changes in levitated fatty acid particles, Atmospheric Chemistry and Physics, 21, 15003-15021, 10.5194/acp-21-15003-2021, 2021.

Mutneja, A. and Karmakar, S.: Length-scale dependence of Stokes-Einstein breakdown in active glass-forming liquids, Physical Review E, 111, 10.1103/PhysRevE.111.035409, 2025.

Nawar, W. W.: Thermal degradation of lipids, J Agr Food Chem, 17, 18-21, 10.1021/jf60161a012, 1969.

Nolte, C. G., Schauer, J. J., Cass, G. R., and Simoneit, B. R. T.: Highly Polar Organic Compounds Present in Meat Smoke, Environmental Science & Technology, 33, 3313-3316, 10.1021/es990122v, 1999.

Pankow, J. F.: An absorption model of the gas/aerosol partitioning involved in the formation of secondary organic aerosol, Atmospheric Environment, 28, 189-193, https://doi.org/10.1016/1352-2310(94)90094-9, 1994.

Pankow, J. F. and Asher, W. E.: SIMPOL.1: a simple group contribution method for predicting vapor pressures and enthalpies of vaporization of multifunctional organic compounds, Atmos. Chem. Phys., 8, 2773-2796, 10.5194/acp-8-2773-2008, 2008.

Pastore, R., Kikutsuji, T., Rusciano, F., Matubayasi, N., Kim, K., and Greco, F.: Breakdown of the Stokes-Einstein relation in supercooled liquids: A cage-jump perspective, Journal of Chemical Physics, 155, 10.1063/5.0059622, 2021.

Patrikios, I. S., Britton, O., Bing, D. K., and Russell, C. S.: Heating unsaturated fatty acids in air produces hemagglutinins, Biochim. Biophys. Acta Lipids Lipid Metab., 1212, 225-234, 10.1016/0005-2760(94)90257-7, 1994.

Peng, Z. and Jimenez, J. L.: Radical chemistry in oxidation flow reactors for atmospheric chemistry research, Chem Soc Rev, 49, 2570-2616, 10.1039/c9cs00766k, 2020.

Peng, Z., Day, D. A., Ortega, A. M., Palm, B. B., Hu, W., Stark, H., Li, R., Tsigaridis, K., Brune, W. H., and Jimenez, J. L.: Non-OH chemistry in oxidation flow reactors for the study of atmospheric chemistry systematically examined by modeling, Atmos. Chem. Phys., 16, 4283-4305, 10.5194/acp-16-4283-2016, 2016.

Preston, T. C.: Non-Fickian diffusion in viscous aerosol particles, Canadian Journal of Chemistry, 100, 168-174, 10.1139/cjc-2021-0187, 2022.

Preston, T. C. and Zuend, A.: Equilibration times in viscous and viscoelastic aerosol particles, Environmental Science: Atmospheres, 2, 1376-1388, 10.1039/d2ea00065b, 2022.

Qian, B., Zhu, X., Su, C., Li, H., Wu, Q., Liu, C., Pan, Y., and Han, B.: Mechanism of Water-Enhanced Volatile Aldehyde Release in Oil Fumes from Thermal Oxidation of Oleic Acid: Insights from Synchrotron Radiation Photoionization and Gas Chromatography–Mass Spectrometry, Molecules, 31, 10.3390/molecules31040594, 2026.

Reyes-Villegas, E., Bannan, T., Le Breton, M., Mehra, A., Priestley, M., Percival, C., Coe, H., and Allan, J. D.: Online Chemical Characterization of Food-Cooking Organic Aerosols: Implications for Source Apportionment, Environ Sci Technol, 52, 5308-5318, 10.1021/acs.est.7b06278, 2018.

Rogge, W. F., Hildemann, L. M., Mazurek, M. A., Cass, G. R., and Simoneit, B. R. T.: Sources of fine organic aerosol. 1. Charbroilers and meat cooking operations, Environmental Science & Technology, 25, 1112-1125, 10.1021/es00018a015, 1991.

Schervish, M. and Shiraiwa, M.: Impact of phase state and non-ideal mixing on equilibration timescales of secondary organic aerosol partitioning, Atmospheric Chemistry and Physics, 23, 221-233, 10.5194/acp-23-221-2023, 2023.

Schmedding, R., Franssen, M., and Zuend, A.: A Machine Learning Approach for Predicting the Pure-Component Surface Tension of Atmospherically Relevant Organic Compounds, ACS ES&T air, 2, 808-823, 10.1021/acsestair.4c00291, 2025.

Shilling, J. E., Zawadowicz, M. A., Liu, J., Zaveri, R. A., and Zelenyuk, A.: Photochemical Aging Alters Secondary Organic Aerosol Partitioning Behavior, ACS Earth and Space Chemistry, 3, 2704-2716, 10.1021/acsearthspacechem.9b00248, 2019.

Shiraiwa, M. and Pöschl, U.: Mass accommodation and gas–particle partitioning in secondary organic aerosols: dependence on diffusivity, volatility, particle-phase reactions, and penetration depth, Atmospheric Chemistry and Physics, 21, 1565-1580, 10.5194/acp-21-1565-2021, 2021.

Shiraiwa, M., Pfrang, C., Koop, T., and Pöschl, U.: Kinetic multi-layer model of gas-particle interactions in aerosols and clouds (KM-GAP): linking condensation, evaporation and chemical reactions of organics, oxidants and water, Atmospheric Chemistry and Physics, 12, 2777-2794, 10.5194/acp-12-2777-2012, 2012.

Song, K., Tang, R., Li, A., Wan, Z., Zhang, Y., Gong, Y., Lv, D., Lu, S., Tan, Y., Yan, S., Yan, S., Zhang, J., Fan, B., Chan, C. K., and Guo, S.: Particulate organic emissions from incense-burning smoke: Chemical compositions and emission characteristics, Science of The Total Environment, 897, 10.1016/j.scitotenv.2023.165319, 2023.

Song, K., Guo, S., Gong, Y. Z., Lv, D. Q., Zhang, Y., Wan, Z. C., Li, T. Y., Zhu, W. F., Wang, H., Yu, Y., Tan, R., Shen, R. Z., Lu, S. H., Li, S. D., Chen, Y. F., and Hu, M.: Impact of cooking style and oil on semi-volatile and intermediate volatility organic compound emissions from Chinese domestic cooking, Atmospheric Chemistry and Physics, 22, 9827-9841, 10.5194/acp-22-9827-2022, 2022.

Sun, P., Liu, Y., Li, Y., Nie, W., Chi, X., Xu, Z., Zhong, S., and Yu, J.: Unified Source Apportionment of Organic Aerosols and Volatile Organic Compounds Reveals Underestimated Cooking Impacts in Urban Air Quality, Am. Chem. Soc. Environ. Sci. Technol. Air., 3, 73-82, 10.1021/acsestair.5c00210, 2026.

Takhar, M., Li, Y., and Chan, A. W. H.: Characterization of secondary organic aerosol from heated-cooking-oil emissions: evolution in composition and volatility, Atmospheric Chemistry and Physics, 21, 5137-5149, 10.5194/acp-21-5137-2021, 2021.

Takhar, M., Stroud, C. A., and Chan, A. W. H.: Volatility Distribution and Evaporation Rates of Organic Aerosol from Cooking Oils and their Evolution upon Heterogeneous Oxidation, ACS Earth and Space Chemistry, 3, 1717-1728, 10.1021/acsearthspacechem.9b00110, 2019.

Takhar, M., Li, Y., Ditto, J. C., and Chan, A. W. H.: Formation pathways of aldehydes from heated cooking oils, Environ Sci Process Impacts, 10.1039/d1em00532d, 2022.

Tan, R., Guo, S., Lu, S., Wang, H., Zhu, W., Yu, Y., Tang, R., Shen, R., Song, K., Lv, D., Zhang, W., Zhang, Z., Shuai, S., Li, S., Chen, Y., and Ding, Y.: Characteristics and Secondary Organic Aerosol Formation of Volatile Organic Compounds from Vehicle and Cooking Emissions, Atmosphere-Basel, 14, 10.3390/atmos14050806, 2023.

Tikkanen, I. P., Buchholz, A., Ylisirniö, A., Schobesberger, S., Virtanen, A., and Yli-Juuti, T.: Comparing secondary organic aerosol (SOA) volatility distributions derived from isothermal SOA particle evaporation data and FIGAERO-CIMS measurements, Atmospheric Chemistry and Physics, 20, 10441-10458, 10.5194/acp-20-10441-2020, 2020.

Wang, H., Guo, S., Yu, Y., Shen, R., Zhu, W., Tang, R., Tan, R., Liu, K., Song, K., Zhang, W., Zhang, Z., Shuai, S., Xu, H., Zheng, J., Chen, S., Li, S., Zeng, L., and Wu, Z.: Secondary aerosol formation from a Chinese gasoline vehicle: Impacts of fuel (E10, gasoline) and driving conditions (idling, cruising), Sci Total Environ, 795, 10.1016/j.scitotenv.2021.148809, 2021.

Wang, X., Chen, Y., Wang, F., Lu, Y., Huang, Z., Wang, W., Wang, Y., and Li, J.: Effects of ammonium sulfate on the hygroscopic properties and phase transition of aerosols with organic surrogates related to biomass burning and atmospheric oxidation, Atmospheric Research, 329, 10.1016/j.atmosres.2025.108464, 2026.

West, C. P., Hsu, Y.-J., MacFeely, K. T., Huston, S. M., Aridjis-Olivos, B. P., Morales, A. C., and Laskin, A.: Volatility Measurements of Individual Components in Organic Aerosol Mixtures Using Temperature-Programmed Desorption–Direct Analysis in Real Time–High Resolution Mass Spectrometry, Analytical Chemistry, 95, 7403-7408, 10.1021/acs.analchem.3c00923, 2023.

Xiao, L., Wang, S., Wang, Y., Wang, B., Ji, C., Lin, X., Liang, H., Zhang, S., Xu, X., and Dong, L.: Density functional theory studies on the oleic acid thermal oxidation into volatile compounds, Food Chem. X, 19, 10.1016/j.fochx.2023.100737, 2023.

Yang, Y., Yang, L., Zheng, M., Cao, D., and Liu, G.: Data acquisition methods for non-targeted screening in environmental analysis, TrAC Trends in Analytical Chemistry, 160, 10.1016/j.trac.2023.116966, 2023.

Yao, Y., Qiang, Z., Zhang, M., Lin, J., and Li, C.: Thermal oxidation mechanism of palmitic aicd, Food Research International, 186, 114372, https://doi.org/10.1016/j.foodres.2024.114372, 2024.

Ye, L., Zhang, F., Zhang, L., and Qi, F.: Theoretical studies on the unimolecular decomposition of propanediols and glycerol, Journal of Physical Chemistry A, 116, 4457-4465, 10.1021/jp301424k, 2012.

Ylisirniö, A., Barreira, L. M. F., Pullinen, I., Buchholz, A., Jayne, J., Krechmer, J. E., Worsnop, D. R., Virtanen, A., and Schobesberger, S.: On the calibration of FIGAERO-ToF-CIMS: importance and impact of calibrant delivery for the particle-phase calibration, Atmospheric Measurement Techniques, 14, 355-367, 10.5194/amt-14-355-2021, 2021.

Ylisirniö, A., Hyttinen, N., Li, Z., Alton, M. W., Nissinen, A., Pullinen, I., Miettinen, P., Yli-Juuti, T., and Schobesberger, S.: The saturation vapor pressures of higher-order polyethylene glycols and achieving a wide calibration range for volatility measurements by FIGAERO-CIMS, Atmospheric Measurement Techniques, 18, 6449-6464, 10.5194/amt-18-6449-2025, 2025.

Yu, Y., Guo, S., Wang, H., Shen, R. Z., Zhu, W. F., Tan, R., Song, K., Zhang, Z. R., Li, S. D., Chen, Y. F., and Hu, M.: Importance of Semivolatile/Intermediate-Volatility Organic Compounds to Secondary Organic Aerosol Formation from Chinese Domestic Cooking Emissions, Environ Sci Tech Let, 9, 507-512, 10.1021/acs.estlett.2c00207, 2022.

Zaveri, R. A., Shilling, J. E., Zelenyuk, A., Liu, J., Bell, D. M., D'Ambro, E. L., Gaston, C. J., Thornton, J. A., Laskin, A., Lin, P., Wilson, J., Easter, R. C., Wang, J., Bertram, A. K., Martin, S. T., Seinfeld, J. H., and Worsnop, D. R.: Growth Kinetics and Size Distribution Dynamics of Viscous Secondary Organic Aerosol, Environmental Science & Technology, 52, 1191-1199, 10.1021/acs.est.7b04623, 2018.

Zeng, J., Yu, Z., Mekic, M., Liu, J., Li, S., Loisel, G., Gao, W., Gandolfo, A., Zhou, Z., Wang, X., Herrmann, H., Gligorovski, S., and Li, X.: Evolution of Indoor Cooking Emissions Captured by Using Secondary Electrospray Ionization High-Resolution Mass Spectrometry, Environmental Science & Technology Letters, 7, 76-81, 10.1021/acs.estlett.0c00044, 2020.

Zhang, D., Cao, Y., Zhang, P., Liang, J., Xue, K., Xia, Y., and Qi, Z.: Investigation of the thermal decomposition mechanism of glycerol: The combination of a theoretical study based on the Minnesota functional and experimental support, Physical Chemistry Chemical Physics, 23, 20466-20477, 10.1039/d1cp01526e, 2021.

Zhang, H., Yee, L. D., Lee, B. H., Curtis, M. P., Worton, D. R., Isaacman-VanWertz, G., Offenberg, J. H., Lewandowski, M., Kleindienst, T. E., Beaver, M. R., Holder, A. L., Lonneman, W. A., Docherty, K. S., Jaoui, M., Pye, H. O. T., Hu, W., Day, D. A., Campuzano-Jost, P., Jimenez, J. L., Guo, H., Weber, R. J., de Gouw, J., Koss, A. R., Edgerton, E. S., Brune, W., Mohr, C., Lopez-Hilfiker, F. D., Lutz, A., Kreisberg, N. M., Spielman, S. R., Hering, S. V., Wilson, K. R., Thornton, J. A., and Goldstein, A. H.: Monoterpenes are the largest source of summertime organic aerosol in the southeastern United States, Proc Natl Acad Sci U S A, 115, 2038-2043, 10.1073/pnas.1717513115, 2018.

Zhang, J., Zuend, A., Top, J., Surdu, M., Haddad, I. E., Slowik, J. G., Prevot, A. S. H., and Bell, D. M.: Estimation of the Volatility and Apparent Activity Coefficient of Levoglucosan in Wood-Burning Organic Aerosols, Environmental Science & Technology Letters, 11, 1214-1219, 10.1021/acs.estlett.4c00608, 2024.

Zhang, X., Pandis, S. N., and Seinfeld, J. H.: Diffusion-Limited Versus Quasi-Equilibrium Aerosol Growth, Aerosol Science and Technology, 46, 874-885, 10.1080/02786826.2012.679344, 2012.

Zhang, Z., Zhu, W., Hu, M., Wang, H., Chen, Z., Shen, R., Yu, Y., Tan, R., and Guo, S.: Secondary Organic Aerosol from Typical Chinese Domestic Cooking Emissions, Environmental Science & Technology Letters, 8, 24-31, 10.1021/acs.estlett.0c00754, 2020.

Zhang, Z., Zhu, W., Hu, M., Wang, H., Tang, L., Hu, S., Shen, R., Yu, Y., Song, K., Tan, R., Chen, Z., Chen, S., Canonaco, F., Prévôt, A. S. H., and Guo, S.: Secondary organic aerosol formation in China from urban-lifestyle sources: Vehicle exhaust and cooking emission, Science of the Total Environment, 857, 10.1016/j.scitotenv.2022.159340, 2023.

Zhao, Y., Hu, M., Slanina, S., and Zhang, Y.: Chemical Compositions of Fine Particulate Organic Matter Emitted from Chinese Cooking, Environmental Science & Technology, 41, 99-105, 10.1021/es0614518, 2007.

Zhou, Z., Li, Y. L., Zhao, F., Xin, R., Huang, X. H., Zhang, Y. Y., Zhou, D., and Qin, L.: Unraveling the Thermal Oxidation Products and Peroxidation Mechanisms of Different Chemical Structures of Lipids: An Example of Molecules Containing Oleic Acid, J Agr Food Chem, 70, 16410-16423, 10.1021/acs.jafc.2c06221, 2022.

Zhu, W., Guo, S., Zhang, Z., Wang, H., Yu, Y., Chen, Z., Shen, R., Tan, R., Song, K., Liu, K., Tang, R., Liu, Y., Lou, S., Li, Y., Zhang, W., Zhang, Z., Shuai, S., Xu, H., Li, S., Chen, Y., Hu, M., Canonaco, F., and Prévôt, A. S. H.: Mass spectral characterization of secondary organic aerosol from urban cooking and vehicular sources, Atmos. Chem. Phys., 21, 15065-15079, 10.5194/acp-21-15065-2021, 2021.

Zuend, A. and Seinfeld, J. H.: Modeling the gas-particle partitioning of secondary organic aerosol: the importance of liquid-liquid phase separation, Atmos. Chem. Phys., 12, 3857-3882, 10.5194/acp-12-3857-2012, 2012.